Journal of Physics A: Mathematical and Theoretical

Appearance of the higher-order Stokes phenomenon in a discrete Airy equation

Journal of Physics A: Mathematical and Theoretical

PAPER

OPEN ACCESS

RECEIVED
27 September 2025

REVISED
9 December 2025

ACCEPTED FOR PUBLICATION
29 December 2025

PUBLISHED
23 January 2026

Appearance of the higher-order Stokes phenomenon in a discrete Airy equation

Aaron J Moston-Duggan[1,*], **Christopher J Howls**[2] **and Christopher J Lustri**[3]

[1] School of Mathematical and Physical Sciences, Macquarie University, Sydney, New South Wales 2109, Australia
[2] Mathematical Sciences, University of Southampton, Highfield, Southampton SO17 1BJ, United Kingdom
[3] School of Mathematics and Statistics, The University of Sydney, Sydney, New South Wales 2006, Australia
[*] Author to whom any correspondence should be addressed.

E-mail: aaron.mostonduggan@hdr.mq.edu.au

Keywords: higher-order Stokes phenomenon, discrete equations, exponential asymptotics

Abstract

We study a discrete variant of the Airy equation and show that discretization produces a more intricate Stokes structure than in the continuous case, inducing the higher-order Stokes phenomenon and infinite accumulations of Stokes and anti-Stokes curves. These features are absent in the continuous Airy equation and are typically seen only in solutions of at least third-order linear homogeneous, second-order or higher linear inhomogeneous, or nonlinear differential equations. Remarkably, this behavior is seen here to arise in a second-order homogeneous linear difference equation. Using exponential asymptotic methods, we derive the asymptotic solutions and the corresponding Stokes structure, with numerical simulations confirming our predictions. We conjecture that the higher order Stokes phenomenon is able to be present in other second order linear difference equations.

1. Introduction

The Stokes phenomenon [1] describes the sudden appearance of exponentially small contributions across Stokes curves in the complex plane. A more recent discovery, the higher-order Stokes phenomenon (HOSP) [2–5], first noted in [6], describes the appearance or termination of Stokes curves at Stokes crossing points (SCPs). In fact, since crossings can only occur when three or more distinct asymptotic contributions are involved, these features are never seen in homogeneous linear second-order differential equations and are usually regarded as higher-order or nonlinear effects. Our results reveal a striking fact: that a HOSP and Stokes curve accumulations may occur in a linear discretization of a *second-order* homogeneous linear differential equation.

The Airy function that decays exponentially as $x \to +\infty$ is the original, and canonical, example of the Stokes phenomenon [1] and has a well-known Stokes curve structure. A scaled version of the function satisfies the singularly perturbed continuous Airy equation

$$\epsilon^2 \frac{\mathrm{d}^2 y}{\mathrm{d}x^2} - xy = 0 \qquad \text{as} \qquad \epsilon \to 0\,. \tag{1}$$

A discrete variant of this equation may be obtained by applying a second-order central difference to the derivative terms in (1), to obtain

$$\frac{\epsilon^2}{h^2}\left(y_{m+1} - 2y_m + y_{m-1}\right) - x_m y_m = 0 \quad \text{as} \quad \epsilon \to 0\,, \tag{2}$$

where $0 < \epsilon \ll 1$, and $m \in \mathbb{Z}$ indexes solution values $\underline{y_m}$ defined at points $x_m \in \mathbb{C}$. The lattice spacing $h = x_{m+1} - x_m$, may vary for fixed ϵ and is $\mathcal{O}(\epsilon)$ in our analysis. We will permit the lattice spacing to be complex, so $h \in \mathbb{C}$. We will subsequently refer to (2) as the 'discrete Airy equation'. The discrete Airy

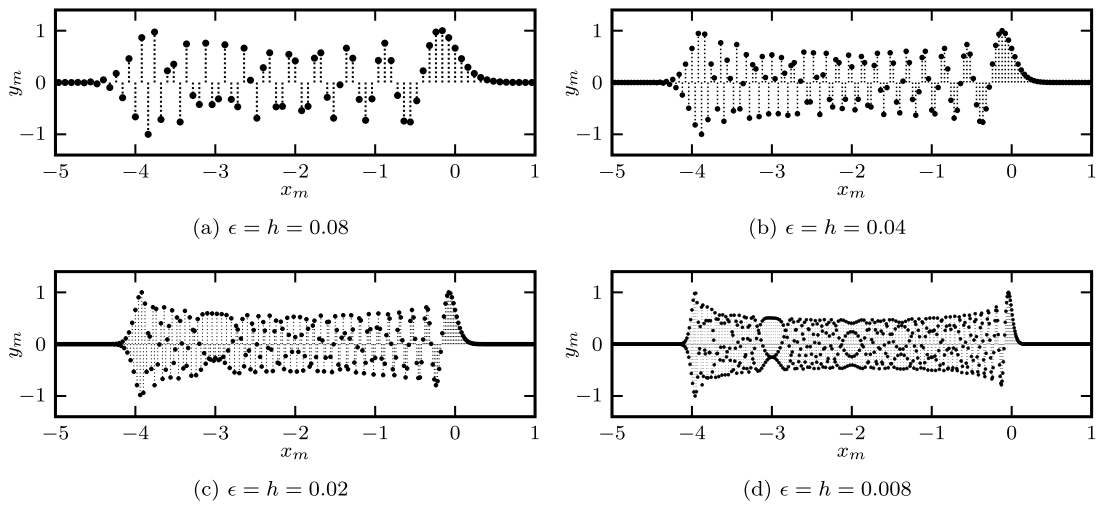

Figure 1. Numerical solutions y_m of the discrete Airy equation (2) along the real axis, which decay as $|x_m| \to \infty$, for several real values of ϵ and h. Each solution is computed with $y_0 = 1$ at $x_0 = -2$ and rescaled so that the maximum value is 1 for comparison. The solutions are oscillatory with slowly varying amplitude between the turning points at $x = 0$ and $x = 4$, and decay exponentially outside this region.

equation arises in implementing transparent boundary conditions [7–10] and non-standard discretization schemes [11, 12] used in numerical studies of wave propagation, including acoustic [7, 9] and electromagnetic [8] waves.

Figure 1 shows numerical solutions to (2) for $y_m \to 0$ as $|x_m| \to \pm\infty$ along the real axis (i.e. $h \in \mathbb{R}$ and $\mathrm{Im}(x_m) = 0$), computed using the method from section 4. These results motivate the present study, revealing a central oscillatory region with slowly varying amplitude bounded by exponentially decaying outer regions. This already contrasts with the solutions of the continuous Airy equation (1), which feature only one oscillatory region and one (growing or decaying) exponential region.

We will derive the corresponding asymptotic solution to the discrete Airy equation (2) and find two turning points at $x = -4$ and $x = 0$. This result will contrast with the continuous Airy equation (1), which has one turning point at $x = 0$. The Stokes phenomenon across these points produces the central oscillatory region shown in figure 1, and the asymptotic results match these numerical solutions.

We will study the transition between the discrete (2) and continuous (1) Airy equations via a continuum approximation to the discrete equation (2) with $x = hm$ and $y(x) = y_m$ to obtain

$$\frac{1}{\sigma^2}\left(y(x+\sigma\epsilon) - 2y(x) + y(x-\sigma\epsilon)\right) - xy(x) = 0 \qquad \text{as} \qquad \epsilon \to 0\,, \tag{3}$$

where $h = \sigma\epsilon$ and $x \in \mathbb{C}$. We refer to (3) as the advance-delay Airy equation, and we determine its asymptotic solutions using the steepest descent method [13]. The advance-delay Airy equation (3) is a continuous equation which, when sampled at discrete points x_m, provides an approximation to the discrete Airy equation (2).

The method of steepest descent [13] is well suited to linear problems, however, unless recast in terms of a Borel transform, it is generally not applicable to nonlinear discrete equations. Instead, such problems may be approached using factorial-over-power methods [14, 15]. We repeat the analysis of (3) in appendix using factorial-over-power methods, and show that it produces identical asymptotic solutions and Stokes structure.

We will show that asymptotic solutions to (2) exhibit the HOSP, despite the fact that a HOSC is generated at a SCP, which requires at least three distinct exponential contributions in order to appear. Furthermore, we will show that the asymptotic solutions contain infinitely many Stokes and anti-Stokes curves accumulating onto limiting curves in the complex plane; this behavior is only seen in equations with an infinite number of distinct exponential contributions, such as nonlinear differential equations. This will be discussed in more detail in section 2.2.

This paper proceeds as follows. In section 2 we provide background on the Stokes phenomenon, the HOSP, and previous work on the asymptotics of discrete equations. In section 3, using the steepest descent method, we derive the asymptotic solutions and the Stokes structure of the advance–delay Airy equation (3). Section 4 presents numerical solutions to the discrete Airy equation (2) and compares them with the asymptotic results of (3) from section 3 and the literature. In section 5, we discuss what

these results imply about the asymptotic behavior of other linear and nonlinear discrete equations and conclude. Appendix reproduces the results of section 3 using the factorial-over-power method, applicable to both linear and nonlinear difference equations.

2. Background and definitions

2.1. Asymptotics of discrete equations

The discrete Airy equation (2) belongs to the class of second-order difference equations, also known as three-term recurrence relations. Such equations appear in special function theory [16, 17], orthogonal polynomials [18–20], random matrix theory [21], quantum mechanics [22], lattice dynamics [23, 24], and topological string theory [25]. These applications have motivated the development of asymptotic methods for discrete systems, broadly classified into two approaches: direct series methods and WKBJ methods.

The series methods developed in [17, 19, 26–30] provide asymptotic solutions to second-order difference equations with linear potentials and coefficients in x_m in the limit $|m| \to \infty$. These approaches extend classical asymptotic methods: see [29, 30] for reviews. The systems considered in these studies contain two special points in x_m, termed turning points by analogy with WKBJ theory [13]. In each of these problems it is possible to construct solutions which are oscillatory with a slowly varying envelope between the turning points, while outside this region they grow or decay exponentially [17, 19, 26, 27].

WKBJ methods for second-order difference equations have been developed using discrete and continuous approaches. Studies such as [31, 32] provide a background of these approaches and propose a unified framework bridging the two. These results are rigorously developed in [33, 34], where asymptotic error bounds are derived. As in the series solutions, the WKBJ solutions predict two turning points for linear second-order difference equations. Discrete versions of more advanced WKBJ methods, such as complex and exact WKBJ, have been explored in, for example, [23, 25, 35] and allow asymptotic analysis of discrete equations with complex domains.

The studies [9, 12, 36] use classical asymptotic methods that apply to the discrete Airy equation (2) only under specific restrictions on variables and parameters. The studies [9, 12] derive asymptotic solutions to (2) as $m \to \infty$ for $\epsilon = 1$ and $x_m = hm$, while [9, 36] obtain additional solutions. The authors in [30, 37] discuss these works, noting that they may be incomplete, and the authors of [9] discuss inconsistencies between the asymptotic results in [9, 12, 36].

These prior studies identify some aspects of the Stokes phenomenon in second-order difference equations, but do not capture the complete Stokes structure. Our results will build on these ideas by providing a complete picture of the Stokes structure, including the HOSP. By studying the asymptotic structure of solutions to (2) in the complex plane, and the Stokes phenomenon that they contain, we will reveal the previously unidentified significance of the HOSP, and explain the significance of this behavior on asymptotic solutions to (2).

More generally, the HOSP has previously been identified in discrete equations that were not obtained from discretization, such as the discrete functional equation that generates the gamma function [38–40]. Our results will suggest that the appearance of the HOSP is *generic* in discretizations of continuous differential equations, even if such behavior cannot exist in the solution to the original continuous equation, as is the case for linear homogeneous second-order differential equations like the Airy equation.

2.2. The Stokes and higher-order Stokes phenomenon

A Stokes phenomenon may occur between pairs of exponential contributions with distinct exponents ϕ_i and ϕ_j, across *Stokes curves* $\mathcal{S}$ in the complex plane, defined by

$$\mathcal{S} = \left\{ x \in \mathbb{C} \,\middle|\, \mathrm{Im}\left(\phi_i - \phi_j\right) = 0 \right\}. \tag{4}$$

If $\mathrm{Re}(\phi_i) > \mathrm{Re}(\phi_j)$ as the Stokes curve is crossed, the maximally dominant asymptotic contribution associated with ϕ_i may switch on the subdominant contribution associated with ϕ_j. If this switching occurs when (4) is satisfied, the exponential contributions (and the saddle points that generate them) are described as being *adjacent* and the Stokes curve is *active*. If (4) is satisfied but no switching occurs between ϕ_i and ϕ_j, the two contributions (and the saddle points that generate them) are described as being non-adjacent and the Stokes curve is described as *inactive*.

Anti-Stokes curves $\mathcal{A}$, on which neither contribution dominates, are defined by

$$\mathcal{A} = \left\{ x \in \mathbb{C} \,\middle|\, \mathrm{Re}\left(\phi_i - \phi_j\right) = 0 \right\}. \tag{5}$$

These curves are generally associated with a change in relative dominance between the two exponential contributions.

The HOSP may occur between three exponential contributions with distinct exponents ϕ_i, ϕ_j, and ϕ_k, across a HOSC $\mathcal{H}$ in the complex plane, defined by

$$\mathcal{H} = \left\{ x \in \mathbb{C} \,\middle|\, \mathrm{Im}\left(\frac{\phi_i - \phi_j}{\phi_i - \phi_k}\right) = 0 \right\}. \tag{6}$$

which corresponds to co-linearity of singularities in the Borel plane [2, 3].

A HOSC can be generated at a SCP, where three Stokes curves intersect [3]; such a point is required for the HOSP to occur. Crossing a HOSC alters which exponential contributions are adjacent, and in some cases, leads to the truncation of the ordinary Stokes curves at the SCP. This property of HOSCs is required in order for the asymptotic solution to exhibit monodromy as the solution is continued around the SCP, and hence for the solution to be analytic near this point. See [2–5, 41, 42] for more detailed explanations of the mechanism underlying the HOSP, and the necessity of such curves for monodromy to be preserved around SCPs.

The overall effect of the HOSP is that a Stokes curve may be active (and exhibit Stokes switching) on one side of the SCP, but inactive on the other side (so that no switching occurs). The condition (6) describes a HOSC across which the Stokes curve on which the ϕ_k contribution switches the ϕ_i contribution can terminate at the relevant SCP.

The observation that HOSCs are generated at SCPs is important, as it restricts the appearance of the HOSP to systems with three or more exponential contributions. A homogeneous linear second-order ordinary differential equation, such as the Airy equation, can produce at most two such contributions and therefore cannot exhibit the HOSP. In general, the presence of three distinct exponential contributions instead requires a differential equation that is homogeneous and third-order (or higher) [43–45], inhomogeneous and second-order (or higher) [4, 46], nonlinear [44, 45, 47], or partial [3, 47, 48].

Olde Daalhuis [46] provided a simple example illustrating how three exponential contributions can arise in an *inhomogeneous* second-order linear differential equation with one contribution from the particular integral and two from the complementary functions. This study calculated the associated Stokes constants, and demonstrated the activation and deactivation of Stokes curves on either side of the SCP through a careful examination of the late-term structure and an analysis of the integration constants appearing in the recurrence relations that generate these terms.

Finally, another significant feature typically associated with nonlinear equations is *Stokes curve accumulation*, where infinitely many Stokes and anti-Stokes curves accumulate onto limiting curves in the complex plane. This asymptotic behavior requires interactions to occur between an infinite number of exponential contributions, which are generic in nonlinear differential equations [44, 45, 47] but cannot occur in linear homogeneous differential equations of any finite order.

2.3. Stokes phenomenon in the Airy equation

A classic example of the Stokes phenomenon occurs in the solutions of the continuous Airy equation (1), whose solutions are the Airy functions Ai and Bi [49]. The general solution of (1) is

$$y = C_1 \,\mathrm{Ai}\left(\epsilon^{-2/3} x\right) + C_2 \,\mathrm{Bi}\left(\epsilon^{-2/3} x\right), \tag{7}$$

where C_1 and C_2 are arbitrary constants and $\mathrm{Ai}(x)$ and $\mathrm{Bi}(x)$ are linearly independent solutions.

Applying the steepest descent method [13] to the continuous Airy equation (1) produces an asymptotic solution that matches the general solution (7) for $C_2 = 0$ and $C_3 = C_1 \epsilon^{2/3}$, where the asymptotic solution has the exponential contributions

$$y_1 \sim \frac{-\mathrm{i}C_3}{2\sqrt{\pi\epsilon}x^{1/4}} \mathrm{e}^{2x^{3/2}/3} \quad \text{and} \quad y_2 \sim \frac{C_3}{2\sqrt{\pi\epsilon}x^{1/4}} \mathrm{e}^{-2x^{3/2}/3} \quad \text{as} \quad \epsilon \to 0. \tag{8}$$

From (8) we observe that $\phi_1 = 2x^{3/2}/3$ and $\phi_2 = -2x^{3/2}/3$. Using (4) and (5), we obtain the Stokes structure shown schematically in figure 2, which contains the Stokes curves, the anti-Stokes curves, and a description of the asymptotic contributions y_1 and y_2 (8) in each region of the complex x-plane. As the Stokes curves with $\mathrm{Arg}(x) = \pm 2\pi/3$ are crossed from right to left, the y_2 contribution switches on the y_1 contribution.

Finally, since the asymptotic behavior in (8) only possesses two exponential contributions, ϕ_1 and ϕ_2, the asymptotic solution does not contain any HOSCs. For such behavior to be present in the solution, a third exponential contribution is required for condition (6) to be satisfied.

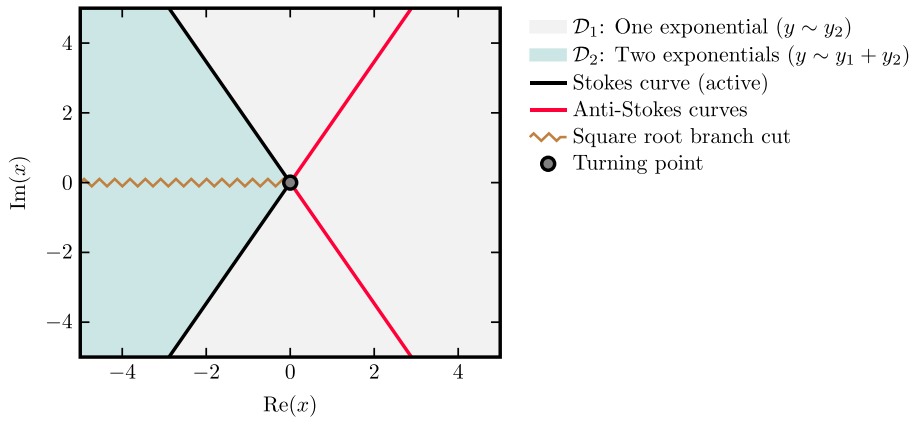

Figure 2. Stokes structure of the Ai solution to the Airy equation (1). Stokes (black) and anti-Stokes (red) curves emerge from the turning point at $x = 0$. In region $\mathcal{D}_1$, the solution has a single decaying exponential as $x \to \infty$ on the real axis. Crossing the anti-Stokes curve causes this contribution to grow instead of decay. Crossing the Stokes curve into $\mathcal{D}_2$ causes a second exponential contribution to appear, resulting in oscillatory behavior on the negative real axis.

3. Steepest descent analysis of the discrete Airy equation

In this section, we compute asymptotic solutions of the advance-delay Airy equation (3) using the steepest descent method [13], and determine the associated Stokes structure.

The steepest descent method is typically only possible for linear (or linearizable) equations. More general exponential asymptotic methods have been developed for nonlinear equations (e.g. [3, 15, 50, 51]). Appendix illustrates how the factorial-over-power method from [15, 50, 51] can reproduce the results from this section in a fashion that could be applied directly to nonlinear difference equations.

3.1. The steepest descent method

To perform the steepest descent analysis, we apply the Fourier transform (9)

$$\hat{y}(\omega) = \int_{-\infty}^{\infty} y(x)\, \mathrm{e}^{-\mathrm{i}\omega x}\, \mathrm{d}x \quad \text{and} \quad y(x) = \frac{1}{2\pi} \int_{-\infty}^{\infty} \hat{y}(\omega)\, \mathrm{e}^{\mathrm{i}\omega x}\, \mathrm{d}\omega\,, \tag{9}$$

to the advance-delay Airy equation (3) and solve the resulting equations for $\hat{y}$. Setting $z = \sigma\epsilon\omega$ and using the inverse transform on $\hat{y}$, the solution y has the integral representation

$$y = \int_{-\infty}^{\infty} g(x,z)\, \mathrm{e}^{-\phi(x,z)/\epsilon}\, \mathrm{d}z \qquad \text{as} \qquad \epsilon \to 0\,, \tag{10}$$

where

$$g(z) = \frac{C}{2\pi\sigma\epsilon} \quad \text{and} \quad \phi(x,z) = -\frac{\mathrm{i}}{\sigma}\left(zx + \frac{2}{\sigma^2}\left(z + \mathrm{i}\sinh(\mathrm{i}z)\right)\right). \tag{11}$$

Here, C is an arbitrary constant. The exact solution (10) is a Laplace-type integral, to which we can apply the steepest descent method to determine asymptotic solutions as $\epsilon \to 0$.

3.1.1. Saddle point locations

The saddle points of (10) satisfy

$$\frac{\partial\phi(x,z_s)}{\partial z} = 0 \quad \text{and} \quad \frac{\partial^2\phi(x,z_s)}{\partial z^2} \neq 0\,, \tag{12}$$

which yields from (11) an infinite number of saddle points located at

$$z_s^- = -\mathrm{i}\cosh^{-1}\left(1 + \frac{\sigma^2 x}{2}\right) + 2\pi s \quad \text{and} \quad z_s^+ = \mathrm{i}\cosh^{-1}\left(1 + \frac{\sigma^2 x}{2}\right) + 2\pi s\,, \tag{13}$$

where $s \in \mathbb{Z}$. These saddle points can be grouped into two sets; z_s^+ in the upper-half z-plane and z_s^- in the lower-half z-plane.

We must specify the branch structure of (13). The inverse hyperbolic cosine can be expressed as

$$\cosh^{-1}\left(1+\frac{\sigma^2 x}{2}\right)=\log\left(1+\frac{\sigma^2 x}{2}+\frac{1}{2}\sqrt{\sigma^2 x}\sqrt{4+\sigma^2 x}\right), \tag{14}$$

which has branch points at $x=-4/\sigma^2$ and $x=0$. We place the square root branch cut along the real interval $x\in(-4/\sigma^2,0)$; crossing this cut changes the sign of one square root, mapping $z_s^+\mapsto z_s^-$ and vice versa. The logarithmic branch cut lies along $x\in(-\infty,-4/\sigma^2)$; crossing thus cut from above adds $2\pi\mathrm{i}$ to the logarithm, which shifts the saddle point index, such that $z_s^+\mapsto z_{s-1}^+$ and $z_s^-\mapsto z_{s+1}^-$.

3.1.2. Saddle point contributions

Each saddle point $z_s^\pm$ has an associated saddle height that we denote as $\phi_s^\pm$, given by

$$\phi_s^\pm(x):=\phi\left(x,z_s^\pm\right)=-\frac{\mathrm{i}}{\sigma}\left[\left(x+\frac{2}{\sigma^2}\right)\left(\pm\mathrm{i}\cosh^{-1}\left(1+\frac{\sigma^2 x}{2}\right)+2\pi s\right)\mp\mathrm{i}\sqrt{x(\sigma^2 x+4)}\right], \tag{15}$$

where the upper and lower signs correspond. Throughout the remainder of this section, we use the same subscript and superscript notation to denote quantities associated with the saddle points z_s^- and z_s^+ as defined in (13).

The asymptotic contributions as $\epsilon\to 0$ are found using the saddle point formula from [13] to be

$$y_s^\pm\sim\frac{1}{\sqrt{2\pi\epsilon}x^{1/4}\left(\sigma^2 x+4\right)^{1/4}}\mathrm{e}^{\phi_s^\pm(x)/\epsilon}, \tag{16}$$

where the upper and lower signs correspond. Each contribution $y_s^\pm$ has two singularities; hence, the solution has turning points at $x=-4/\sigma^2$ and $x=0$.

3.1.3. Stokes, anti-Stokes and HOSCs

Using conditions (4) and (5), we introduce specific notation for (possibly inactive) Stokes and anti-Stokes curves caused by interactions between contributions from saddle points $z_s^\pm$. All such pairings can be written as

$$\mathcal{S}_{s,p}^{\pm,\pm}=\left\{x\in\mathbb{C}\,|\,\mathrm{Im}\left(\phi_s^\pm-\phi_p^\pm\right)=0\right\}\quad\text{and}\quad\mathcal{A}_{s,p}^{\pm,\pm}=\left\{x\in\mathbb{C}\,|\,\mathrm{Re}\left(\phi_s^\pm-\phi_p^\pm\right)=0\right\}, \tag{17}$$

where the sign choices on the same side of the equality are independent, but the first sign choice on each side and the second sign choice on each side correspond.

Using condition (6), we introduce notation for the relevant HOSCs, which we denote by

$$\mathcal{H}_{s,s+1,s+1}^{-,+,-}=\left\{x\in\mathbb{C}\,\middle|\,\mathrm{Im}\left(\frac{\phi_s^--\phi_{s+1}^+}{\phi_s^--\phi_{s+1}^-}\right)=0\right\}, \tag{18}$$

$$\mathcal{H}_{s,s,s+1}^{+,-,+}=\left\{x\in\mathbb{C}\,\middle|\,\mathrm{Im}\left(\frac{\phi_s^+-\phi_{s+1}^-}{\phi_s^+-\phi_{s+1}^+}\right)=0\right\}. \tag{19}$$

While other triplets exist, only these HOSCs influence the asymptotic behavior of the solution.

3.2. Detailed analysis for $\sigma=1$

In this section, we determine the Stokes structure and construct the asymptotic solution of the advance-delay Airy equation (3) for the case $\sigma=1$. A schematic of the resulting Stokes structure is shown in figure 3.

The asymptotic solution is an infinite sum of saddle point contributions that depend on the value of x. In region $\mathcal{D}_1$, only the upper saddle points z_s^+ contribute. In region $\mathcal{D}_2$, only the lower saddle points z_s^- contribute. In region $\mathcal{D}_3$, both sets of saddle points, z_s^+ and z_s^-, contribute.

Figure 3 shows the regions $\mathcal{D}_1$, $\mathcal{D}_2$, and $\mathcal{D}_3$, separated by active Stokes curves. The curves $\mathcal{S}_{s,s}^{+,-}$ emanate from $x=0$, while $\mathcal{S}_{s,s+1}^{-,+}$ emanate from $x=-4$. These curves intersect at two SCPs, located at $x\approx-2\pm 3.018\mathrm{i}$. The Stokes curves $\mathcal{S}_{s,s}^{+,-}$ and $\mathcal{S}_{s,s+1}^{-,+}$ become inactive at the SCPs, and do not continue past these points. Additional Stokes curves $\mathcal{S}_{s,s+1}^{-,-}$ and $\mathcal{S}_{s,s+1}^{+,+}$ extend vertically from the SCPs and are inactive between them.

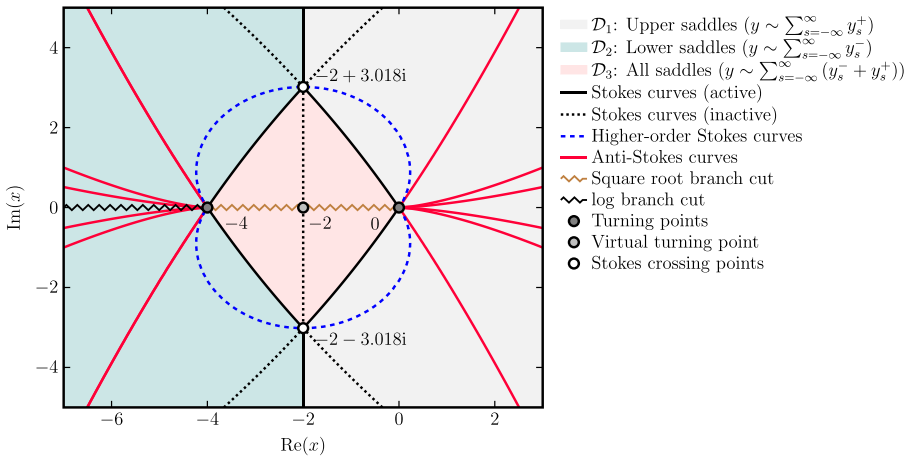

Figure 3. Stokes structure of the advance-delay Airy equation (3) for $\sigma = 1$, with turning points at $x = 0$ and $x = -4$ (gray circles). In region $\mathcal{D}_1$, contributions from upper saddle points z_s^+ are exponentially decaying on the positive real axis but become growing after crossing anti-Stokes curves (red). An infinite number of anti-Stokes curves accumulate near the real axis, each for a different z_s^+ (only the first three are shown). Similar behavior occurs for lower saddle points z_s^- along the negative real axis. Crossing Stokes curves (black) causes contributions to switch on and off. In $\mathcal{D}_2$, contributions from z_s^+ vanish and z_s^- appear. In $\mathcal{D}_3$, all contributions appear. The HOSC (dashed blue) truncate the active Stokes curves at the SCPs (white circles).

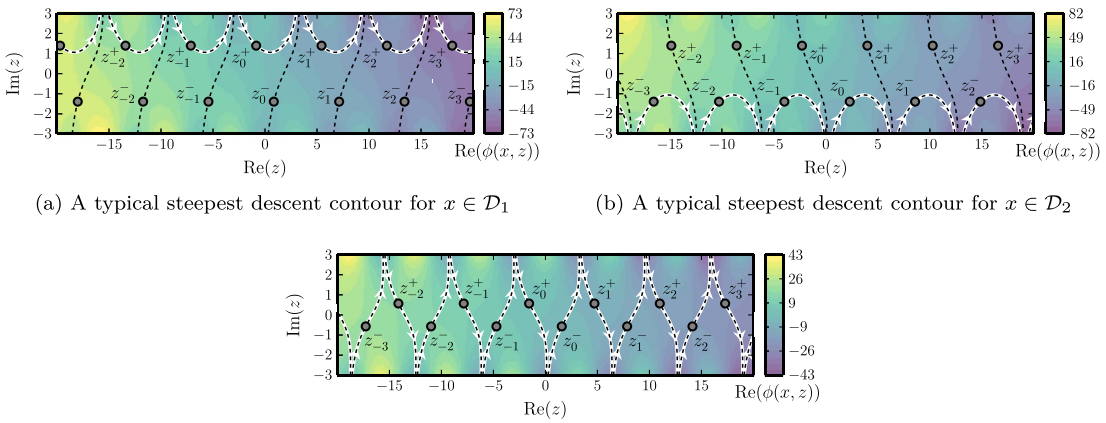

(a) A typical steepest descent contour for $x \in \mathcal{D}_1$

(b) A typical steepest descent contour for $x \in \mathcal{D}_2$

(c) A typical steepest descent contour for $x \in \mathcal{D}_3$

Figure 4. Steepest descent analysis schematics for the advance-delay Airy equation (3) for $\sigma = 1$, showing the steepest descent contour (white), saddle points $z_s^{\pm}$ (circles), and constant phase contours (dashed). Figures (a), (b), and (c) show typical schematics in regions $\mathcal{D}_1$, $\mathcal{D}_2$, and $\mathcal{D}_3$, respectively.

Figure 4 shows typical steepest descent schematics in regions $\mathcal{D}_1$, $\mathcal{D}_2$, and $\mathcal{D}_3$. This analysis reveals that the solution can be written as

$$y \sim \sum_{s=-\infty}^{\infty} \left(c_s^- y_s^- + c_s^+ y_s^+ \right) \quad \text{as} \quad \epsilon \to 0\,, \tag{20}$$

where $c_s^+ = 1$ and $c_s^- = 0$ if $x \in \mathcal{D}_1$, $c_s^+ = 1$ and $c_s^- = 1$ if $x \in \mathcal{D}_2$, and $c_s^+ = 0$ and $c_s^- = 1$ if $x \in \mathcal{D}_3$. These coefficients change across the Stokes curves, which separate the regions $\mathcal{D}_1$, $\mathcal{D}_2$ and $\mathcal{D}_3$.

3.2.1. Steepest descent curves

In this section, we demonstrate how the steepest descent contour varies between regions $\mathcal{D}_1$, $\mathcal{D}_2$ and $\mathcal{D}_3$, to explain the switching behavior observed in figure 3. Taken together, the detailed analysis of this section explains how the asymptotic solution around the SCPs satisfies the monodromy property.

Stokes switching across $\mathcal{S}_{s,s}^{+,-}$: Figure 5 shows how the steepest descent contour changes as the Stokes curves $\mathcal{S}_{s,s}^{+,-}$ are crossed. Following the labeled path from ① to ② to ③, we observe that as the Stokes curves are crossed, each saddle z_s^+ in the upper row switches on a saddle z_s^- in the lower row. Hence,

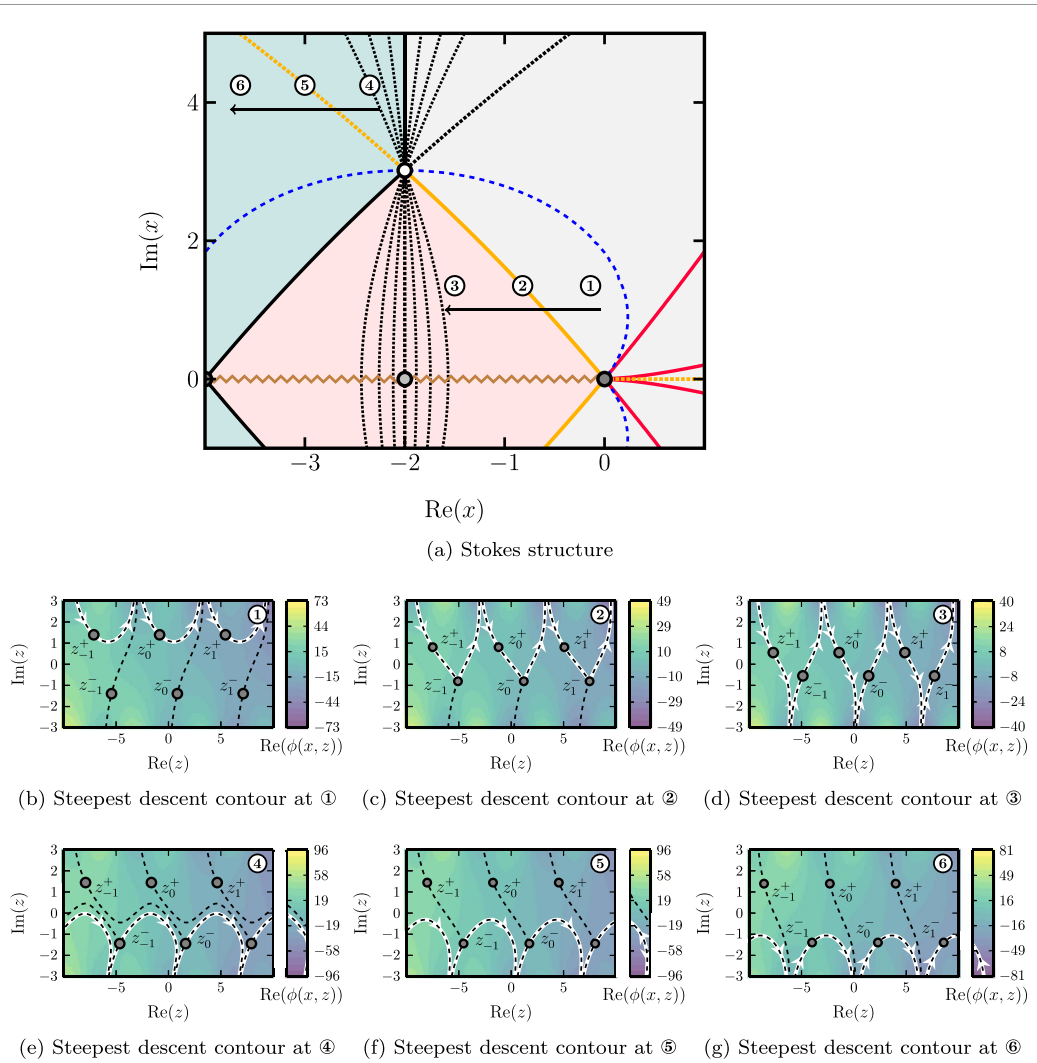

(a) Stokes structure

(b) Steepest descent contour at ① (c) Steepest descent contour at ② (d) Steepest descent contour at ③

(e) Steepest descent contour at ④ (f) Steepest descent contour at ⑤ (g) Steepest descent contour at ⑥

Figure 5. Schematics of Stokes switching for the Stokes curves $\mathcal{S}_{s,s}^{+,-}$ with $\sigma = 1$. (a) Stokes structure schematic. The legend matches that of figure 3, except that we highlight the Stokes curves $\mathcal{S}_{s,s}^{+,-}$ (yellow) and include inactive Stokes curves (dotted yellow and black) to illustrate the Stokes switching behavior. Points ① – ⑥ correspond to the steepest descent schematics shown in (b)–(g). (b)–(g) Steepest descent schematics. The legends match those of figure 4.

additional contributions from the z_s^- saddles emerge in the asymptotic solution as x moves from $\mathcal{D}_1$ to $\mathcal{D}_3$.

Following the path from ④ to ⑤ to ⑥, we see that the Stokes curves $\mathcal{S}_{s,s}^{+,-}$ are inactive in $\mathcal{D}_2$. Although the contributions for the saddles z_s^+ and z_s^- have equal phase at ⑤, the steepest descent contour does not change, so no Stokes switching occurs.

Stokes switching across $\mathcal{S}_{s,s+1}^{-,+}$: Figure 6 shows how the steepest descent contour changes as the Stokes curves $\mathcal{S}_{s,s+1}^{-,+}$ are crossed. Following the labeled path from ① to ② to ③, we observe that as the Stokes curves are crossed, each saddle z_s^- in the lower row switches on a saddle z_{s+1}^+ in the upper row. Hence, additional contributions from the z_s^+ saddles emerge in the asymptotic solution as x moves from $\mathcal{D}_2$ to $\mathcal{D}_3$.

Following the path from ④ to ⑤ to ⑥, we see that the Stokes curves $\mathcal{S}_{s,s+1}^{-,+}$ are inactive in $\mathcal{D}_1$. Although the contributions for the saddles z_s^- and z_{s+1}^+ have equal phase at ⑤, the steepest descent contour does not change, so no Stokes switching occurs.

Stokes switching across $\mathcal{S}_{s,s+1}^{+,+}$ and $\mathcal{S}_{s,s+1}^{-,-}$: Figure 7 shows how the steepest descent contour changes as the Stokes curves $\mathcal{S}_{s,s+1}^{+,+}$ and $\mathcal{S}_{s,s+1}^{-,-}$ are crossed. Following the labeled path from ① to ② to ③, we observe that as the Stokes curves are crossed, each saddle z_s^+ in the upper row switches off and each

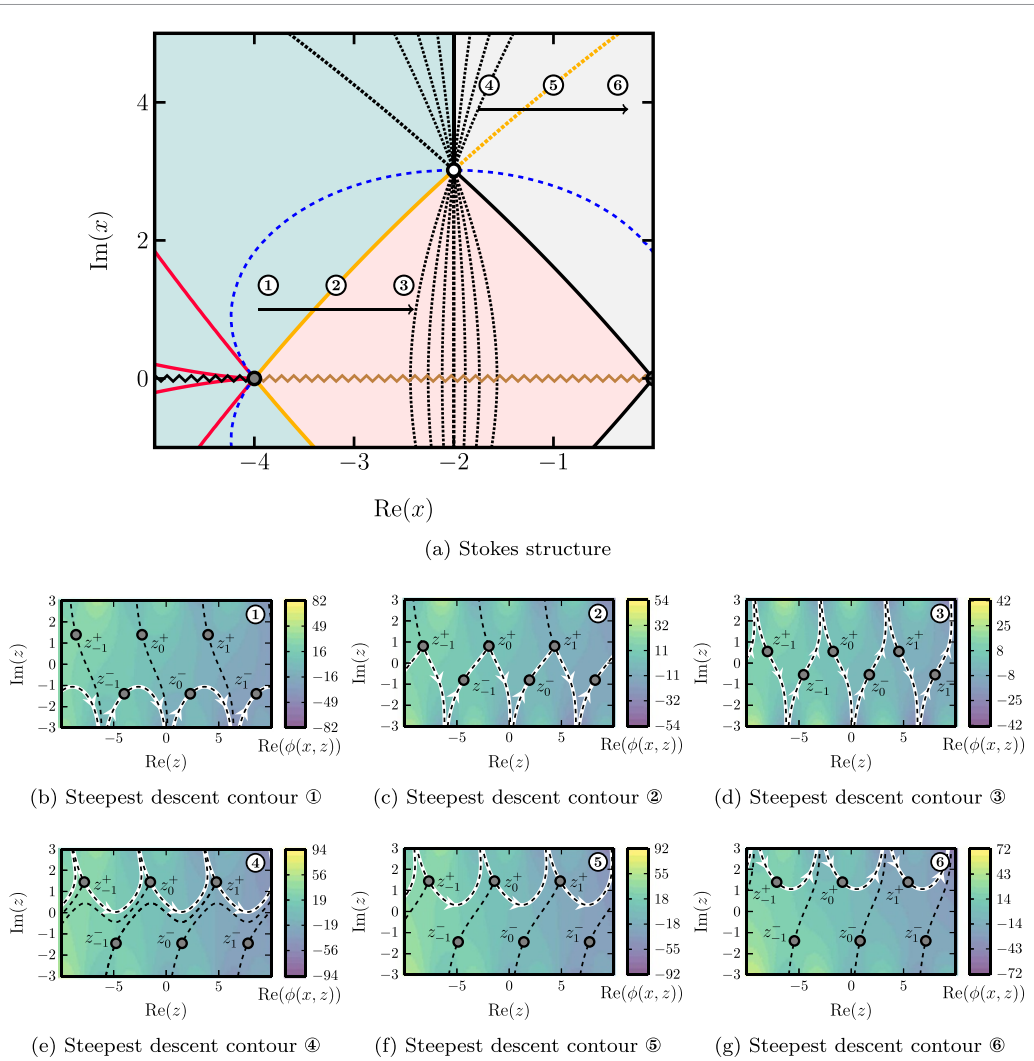

(a) Stokes structure

(b) Steepest descent contour ① (c) Steepest descent contour ② (d) Steepest descent contour ③

(e) Steepest descent contour ④ (f) Steepest descent contour ⑤ (g) Steepest descent contour ⑥

Figure 6. Schematics of Stokes switching for the Stokes curves $\mathcal{S}^{-,+}_{s,s+1}$ with $\sigma = 1$. (a) Stokes structure schematic. The legend matches that of figure 3, except that we highlight the Stokes curves $\mathcal{S}^{-,+}_{s,s+1}$ (yellow) and include inactive Stokes curves (dotted yellow and black) to show the Stokes switching behavior. Points ① – ⑥ correspond to the steepest descent schematics shown in (b)–(g). (b)–(g) Steepest descent schematics. The legends match those of figure 4.

saddle z_s^- in the lower row switches on simultaneously. Hence, contributions from the z_s^- saddles appear and contributions from the z_s^+ saddles disappear from the asymptotic solution as x moves from $\mathcal{D}_1$ to $\mathcal{D}_2$. This unusual switching behavior, in which all saddle contributions switch on or off simultaneously, is caused by the integral endpoint at $z = -\infty$.

Following the path from ④ to ⑤ to ⑥, we see that the Stokes curves $\mathcal{S}^{+,+}_{s,s+1}$ and $\mathcal{S}^{-,-}_{s,s+1}$ are inactive in $\mathcal{D}_3$. Although the contributions from the pairs z_s^- and z_{s+1}^-, and z_s^+ and z_{s+1}^+ have equal phase at ⑤, the steepest descent contour does not change, so no Stokes switching occurs.

Higher-order Stokes phenomenon across $\mathcal{H}^{-,+,-}_{s,s+1,s+1}$ and $\mathcal{H}^{+,-,+}_{s,s,s+1}$: In each of the figures 5–7, the effect of crossing an inactive Stokes curve was shown in (e)–(g). In each case, the condition (4) was satisfied but no switching occurred. This is because the saddles satisfying the condition were adjacent on one side of the SCP, but not adjacent on the other. Such a change in adjacency can only occur across a HOSC; crossing this curve causes the Stokes curves to become inactive so that no switching can occur.

In figures 5–7 the saddle point adjacency changes upon crossing the HOSCs $\mathcal{H}^{-,+,-}_{s,s+1,s+1}$ and $\mathcal{H}^{+,-,+}_{s,s,s+1}$. Stokes switching only occurs between adjacent saddles. Inside the region bounded by these HOSCs, z_s^+ is adjacent to z_s^- and z_{s-1}^-, while z_s^- is adjacent to z_s^+ and z_{s+1}^+, allowing Stokes switching across $\mathcal{S}^{+,-}_{s,s}$ and $\mathcal{S}^{-,+}_{s,s+1}$. Outside this region, z_s^+ is adjacent to z_{s+1}^+ and z_s^- is adjacent to z_{s+1}^-, enabling Stokes switching across $\mathcal{S}^{+,+}_{s,s+1}$ and $\mathcal{S}^{-,-}_{s,s+1}$.

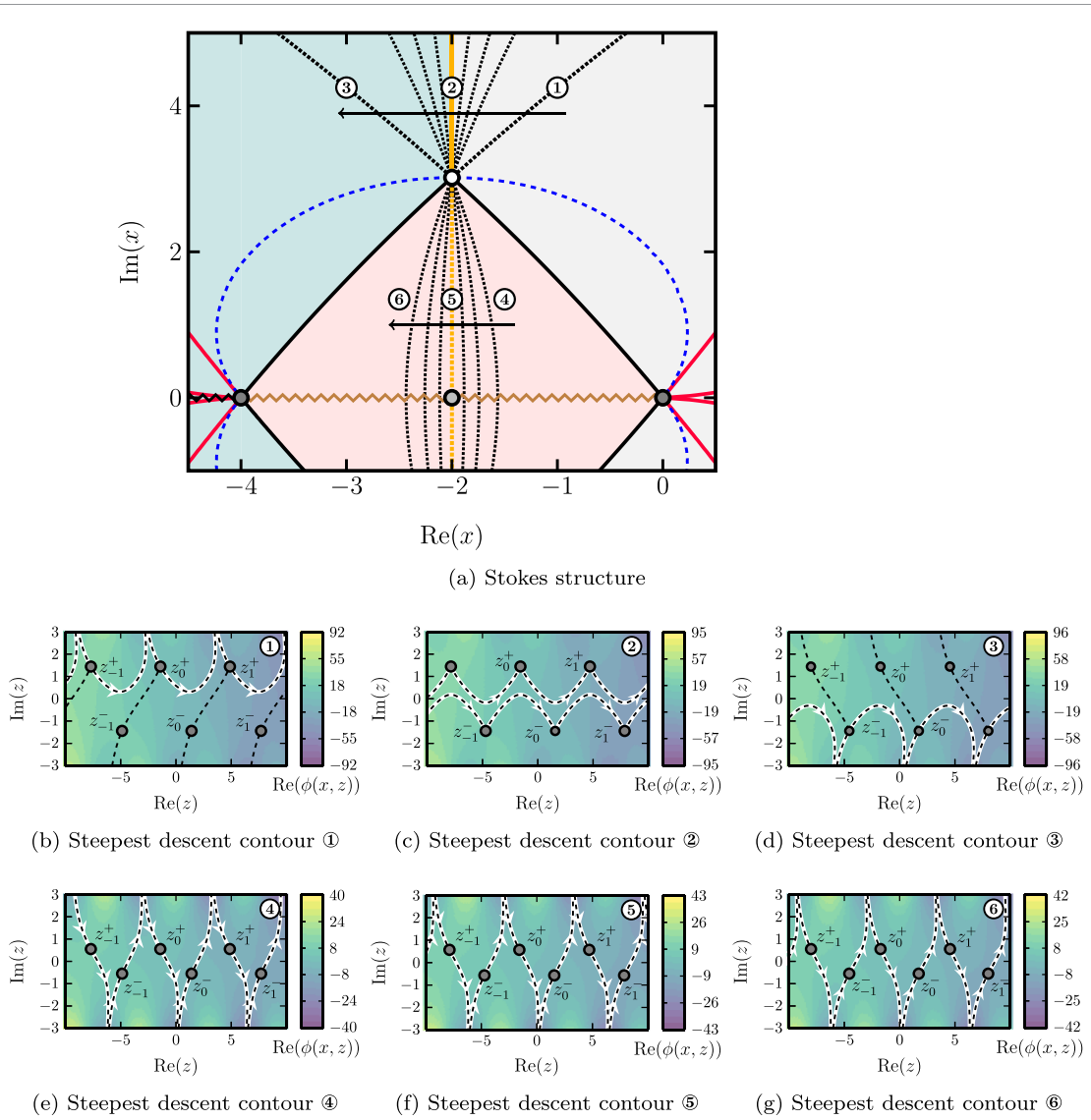

(a) Stokes structure

(b) Steepest descent contour ①

(c) Steepest descent contour ②

(d) Steepest descent contour ③

(e) Steepest descent contour ④

(f) Steepest descent contour ⑤

(g) Steepest descent contour ⑥

Figure 7. Schematics of Stokes switching for the Stokes curves $\mathcal{S}^{+,+}_{s,s+1}$ and $\mathcal{S}^{-,-}_{s,s+1}$ with $\sigma = 1$. (a) Stokes structure schematic. The legend matches that of figure 3, except that we highlight the Stokes curves $\mathcal{S}^{+,+}_{s,s+1}$ and $\mathcal{S}^{-,-}_{s,s+1}$ (yellow) and include inactive Stokes curves (dotted yellow and black) to show the Stokes switching behavior. Points ① – ⑥ correspond to the steepest descent schematics shown in (b)–(g). (b)–(g) Steepest descent schematics. The legends match those of figure 4.

Branch cuts: The branch cuts do not affect which saddles contribute to the asymptotic solution. The logarithmic branch cut along the real axis for $x < -4$, maps $z_s^- \to z_{s+1}^-$; since it is within $\mathcal{D}_2$, all saddles in the lower row contribute. The branch cut along the real axis for $-4 < x < 0$, maps $z_s^- \leftrightarrow z_s^+$; since it is within $\mathcal{D}_3$, all saddles contribute. The branch cuts therefore relabel the contributions but do not alter the asymptotic solution.

3.3. Accumulation of Stokes and anti-Stokes curves

In this section, we comment on an unusual feature, not typically seen in solutions to linear differential equations. The discrete solution contains an infinite number of anti-Stokes curves accumulating towards the real axis and an infinite number of (inactive) Stokes curves accumulating towards $\mathrm{Re}(x) = -2$. These accumulations are illustrated in figure 8.

For $\mathrm{Re}(x) \leqslant 4$, the anti-Stokes curves $\mathcal{A}^{+,-}_{s,s+j}$ with $j \geqslant 1$ accumulate onto the real axis, and for $\mathrm{Re}(x) \geqslant 0$, the curves $\mathcal{A}^{-,+}_{s,s+j}$ with $j \geqslant 1$ accumulate similarly. As the real axis is approached, infinitely many anti-Stokes curves cause the associated saddle point contributions to switch from exponentially large to small. Although these curves do not change the form of the solution (20), they induce a rapid shift in the dominant balance of contributions near the real axis.

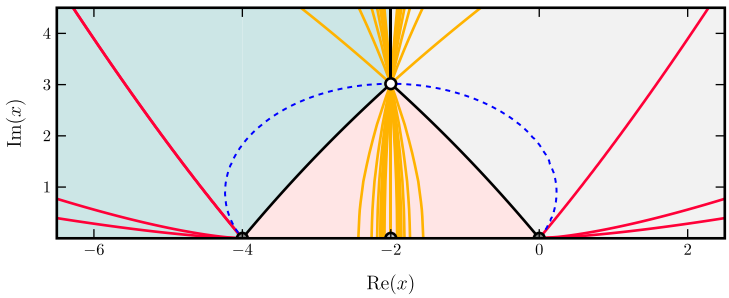

Figure 8. Schematic of inactive Stokes and anti-Stokes curve accumulations for the advance-delay Airy equation (3) for $\sigma = 1$. The legend matches that of figure 3, except that we include the inactive Stokes curves (yellow) to illustrate the accumulations. Anti-Stokes curves accumulate on the real axis for $x > 0$ and $x < -4$, while inactive Stokes curves accumulate toward $\mathrm{Re}(x) = -2$.

The inactive Stokes curves $\mathcal{S}^{-,+}_{s,s+j}$ and $\mathcal{S}^{+,-}_{s,s+j}$ with $j \geqslant 1$ accumulate toward the line $\mathrm{Re}(x) = -2$. Between the SCPs, the Stokes curves $\mathcal{S}^{-,+}_{s,s+j}$ with $j \geqslant 1$ accumulate towards $\mathrm{Re}(x) < -2$ from the left, while the Stokes curves $\mathcal{S}^{+,-}_{s,s+j}$ with $j \geqslant 1$ accumulate towards $\mathrm{Re}(x) < -2$ on the right; the reverse is true outside of the SCPs.

Each inactive Stokes curve corresponds to a pair of saddles with equal phase, but no Stokes switching occurs. As shown in figure 8, approaching the line $\mathrm{Re}(x) = -2$ reveals a sequence of inactive Stokes curves connecting z_s^- to z_{s+2}^+, z_{s+3}^+, and so on. Although these curves do not influence the solution of the discrete Airy equation, the accumulation of infinitely many (even inactive) Stokes curves is an unusual feature in linear problems.

These unusual accumulations occur because the asymptotic solution (20) contains infinitely many saddle point contributions, leading to infinitely many possible Stokes switching interactions and the resulting curve accumulations. In continuous differential equations, such behavior is typically linked to nonlinearity, where the transseries has infinitely many terms [47]. Here, however, it arises in a linear discrete system from the 2π-periodicity of the saddle locations, a generic feature of discrete problems (see, e.g. [16, 24, 50]). In these previous studies, only the Stokes curves associated with the dominant contributions are considered and therefore the accumulations are not identified. Thus, unlike continuous systems, the observed accumulation of Stokes and anti-Stokes curves is not due to nonlinearity, but is instead due to the discretization.

3.4. Varying σ

In section 3.2, we presented the Stokes structure and asymptotic solutions of the advance-delay Airy equation (3) for $\sigma = 1$. Allowing σ to vary allows the spatial step h to change independently of the small parameter ϵ, including the use of spatial steps in a complex direction when σ is complex. This is a useful generalization as many special functions satisfy difference equations from which their asymptotic properties in complex directions can be determined [16, 18–20, 52]. This generalization significantly alters the Stokes structure.

Figure 9 illustrates how $|\sigma|$ affects the Stokes structure. The turning point at $x = 0$ remains fixed, while the other turning and virtual turning points lie at $x = -4/\sigma^2$ and $x = -2/\sigma^2$, respectively. Since active Stokes curves emerge from these points, the Stokes structure scales with $1/|\sigma|^2$, and the regions $\mathcal{D}_1$, $\mathcal{D}_2$, and $\mathcal{D}_3$ scale accordingly. As $|\sigma| \to 0$ the Stokes structure near $x = 0$ approaches that of the continuous Airy equation (1).

While changing $|\sigma|$ results in a straightforward scaling of the Stokes structure, altering $\mathrm{Arg}(\sigma)$ has a more significant impact. Figure 10 illustrates how $\mathrm{Arg}(\sigma)$ affects the Stokes structure. The turning points lie along the ray $\mathrm{Arg}(x) = \pi - 2\mathrm{Arg}(\sigma)$, while the SCPs lie along the rays $\mathrm{Arg}(x + 2/\sigma^2) = \pm(\pi/2 + \mathrm{Arg}(\sigma))$. As $\mathrm{Arg}(\sigma)$ varies, key features of the Stokes structure deform and rotate, and the geometry of the regions $\mathcal{D}_1$, $\mathcal{D}_2$, and $\mathcal{D}_3$ changes accordingly. For $\mathrm{Arg}(\sigma) = (2 + 4n)\pi/2$, with $n \in \{0, 1, 2, 3, 4, 5\}$, each SCP coalesces with a turning point. The active Stokes curves $\mathcal{S}^{+,-}_{s,s}$ and $\mathcal{S}^{-,+}_{s,s+1}$ then coincide, eliminating region $\mathcal{D}_3$. In these cases, only $\mathcal{D}_1$ and $\mathcal{D}_2$ remain, and there is no region in which all contributions are simultaneously present.

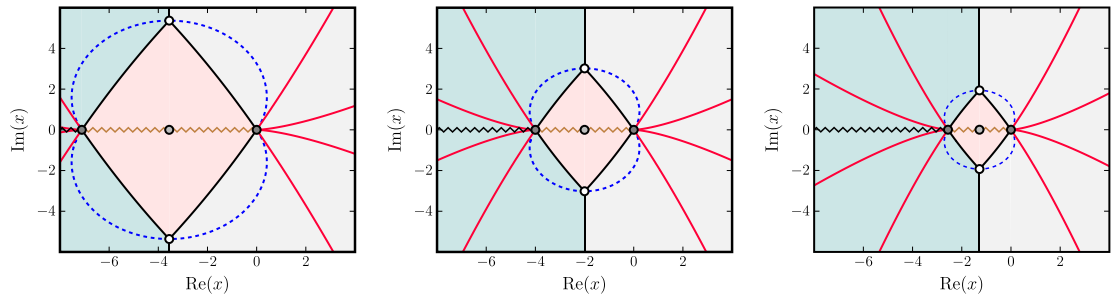

(a) $\sigma = 0.75$ (b) $\sigma = 1$ (c) $\sigma = 1.25$

Figure 9. Schematic showing how $|\sigma|$ affects the Stokes structure. The legend is identical to figure 3. Panels (a)–(c) show the Stokes structure for varying $|\sigma|$ with $\mathrm{Arg}(\sigma) = 0$. The turning point $x = 0$ remains fixed, while the Stokes structure scales with $1/|\sigma|^2$.

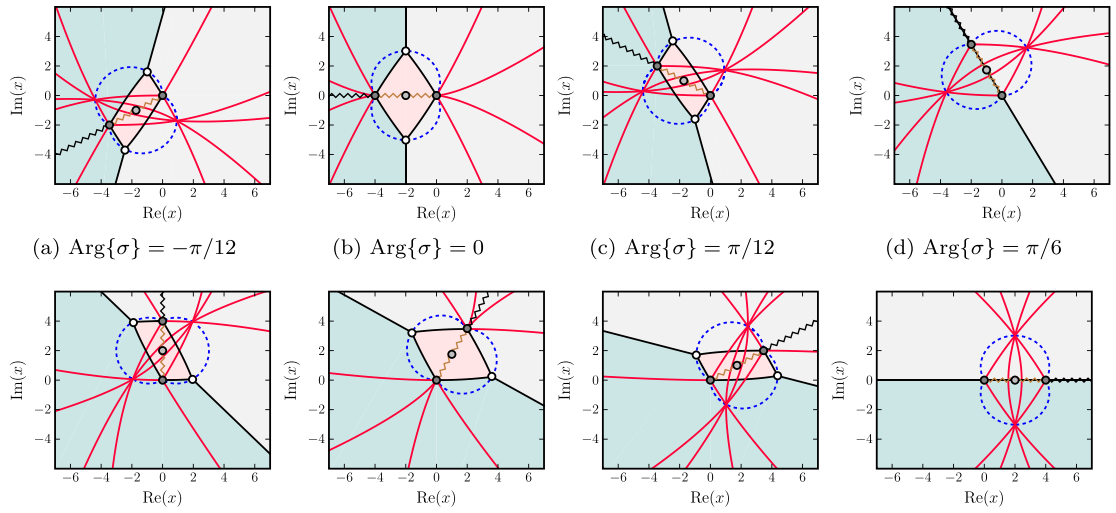

(a) $\mathrm{Arg}\{\sigma\} = -\pi/12$ (b) $\mathrm{Arg}\{\sigma\} = 0$ (c) $\mathrm{Arg}\{\sigma\} = \pi/12$ (d) $\mathrm{Arg}\{\sigma\} = \pi/6$

(e) $\mathrm{Arg}\{\sigma\} = \pi/4$ (f) $\mathrm{Arg}\{\sigma\} = \pi/3$ (g) $\mathrm{Arg}\{\sigma\} = 5\pi/12$ (h) $\mathrm{Arg}\{\sigma\} = \pi/2$

Figure 10. Schematic showing how $\mathrm{Arg}(\sigma)$ affects the Stokes structure. The legend is identical to figure 3. Panels (a)–(h) show the Stokes structure for varying $\mathrm{Arg}(\sigma)$ with $|\sigma| = 1$. The turning point $x = 0$ remains fixed. As $\mathrm{Arg}(\sigma)$ varies, key features of the Stokes structure deform and rotate. The regions $\mathcal{D}_1$, $\mathcal{D}_2$ and $\mathcal{D}_3$ change accordingly.

4. Comparison of results

4.1. Numerical comparison

To validate our asymptotic solutions (20) of the advance-delay Airy equation (3), we compare them with numerical solutions of the discrete Airy equation (2). Solutions of (2) can be written as the matrix system $M\mathbf{y} = \mathbf{0}$, where the only nonzero entries are given by $M_{m-1,m} = 1/\sigma^2$, $M_{m,m} = -2/\sigma^2 - x_m$, $M_{m+1,m} = 1/\sigma^2$, and $\mathbf{y}_m = y_m$. As such, these solutions lie along straight lines x_m in the complex plane, with successive point separated by the complex step $h = \sigma\epsilon$. Since ϵ is real and positive, the complex parameter σ determines the direction of these lines.

We seek decaying solutions such that $y_m \to 0$ as $|x_m| \to \infty$. To approximate the infinite-dimensional system, we truncate the domain to a finite interval $x_m \in [x_{M_1}, x_{M_2}]$, with x_{M_1} and x_{M_2} chosen so that the boundary values are negligibly small. We therefore impose $y_{M_1} = y_{M_2} = 0$, setting a value for y_0, gives a solvable system. To ensure accuracy of the numerical solutions, we solve the system on progressively larger domains until the solution converges.

Figure 1 shows numerical solutions to the discrete Airy equation (2) for $\sigma = 1$ and various values of ϵ. The scheme is implemented with $y_0 = 1$ at $x_0 = -2$, and the solutions are normalized to have a maximum value of 1 for visual clarity. These solutions lie along the real axis of x_m because both σ and x_0 are real valued. The solution is oscillatory between $x \approx -4$ and $x \approx 0$, and decays exponentially outside this region. Near $x = -4$ and $x = 0$, the envelope follows an Airy profile. These features are consistent

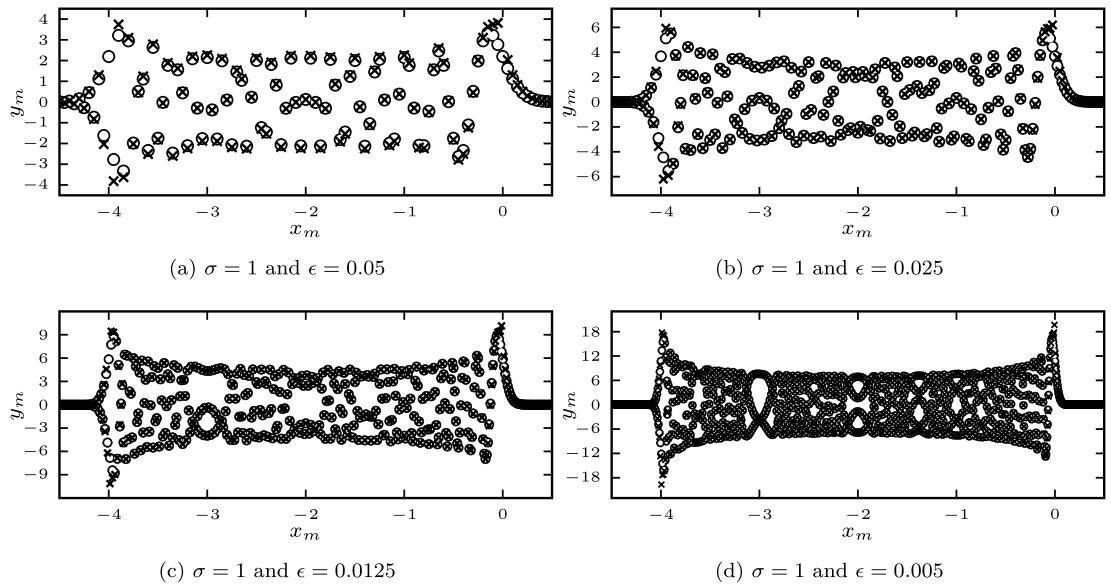

(a) $\sigma = 1$ and $\epsilon = 0.05$ (b) $\sigma = 1$ and $\epsilon = 0.025$

(c) $\sigma = 1$ and $\epsilon = 0.0125$ (d) $\sigma = 1$ and $\epsilon = 0.005$

Figure 11. Asymptotic solutions (20) of the advance-delay Airy equation (3) and numerical solutions of the discrete Airy equation (1) along the real axis, for several values of $(x_m + 2/\sigma^2)/(\sigma\epsilon) \in \mathbb{Z}$. The continuous asymptotic solution is sampled at discrete points x_m. Numerical results (circles) and asymptotic results (crosses) are in agreement, with the accuracy improving as $\epsilon \to 0$. In figures (b), (c), and (d), the solutions are visually indistinguishable except near the turning points.

with the asymptotic prediction that the solution locally resembles Airy function behavior near each turning point.

For certain values of σ, ϵ, h, and x_m, the asymptotic solution simplifies, enabling direct comparison with numerical results. If $(x_m + 2/\sigma^2)/(\sigma\epsilon) \in \mathbb{Z}$ for all m, then the terms y_s^- and y_p^- are identical up to a scalar multiple for all s and p, and similarly for y_s^+ and y_p^+. In this case, the asymptotic solution (20) reduces to

$$y \sim \begin{cases} cy_0^+ & \text{for } x \in \mathcal{D}_1 \\ cy_0^- & \text{for } x \in \mathcal{D}_2 \\ cy_0^- + cy_0^+ & \text{for } x \in \mathcal{D}_3 \end{cases}. \tag{21}$$

Figure 11 shows the numerical solutions of the discrete Airy equation (2) compared to the asymptotic solution (21). The numerical scheme uses the initial condition $y_0 = y(x_0)$ at $x_0 = -2$, where $y_0 = y(x_0)$ is computed from (21) with $c = 1$. Again, these solutions lie along the real axis of x_m because both σ and x_0 are real valued. As $\epsilon \to 0$, the agreement between the numerical and asymptotic solutions improves.

Figure 12 shows numerical solutions y_m of the discrete Airy equation (2), compared with the Stokes structure predicted by our asymptotic solutions (20) to the advance-delay Airy equation (3). The discrete Airy equation (2) describes solutions y_m along a single line x_m in the complex plane, whose orientation is determined by the spatial step $h = \sigma\epsilon$. To illustrate the behavior of the solution throughout the complex plane, rather than along a single line, we compute y_m along multiple such lines x_m. Each line has the same orientation, but they are shifted relative to one another in a direction perpendicular to their common orientation.

For each line x_m, the numerical scheme is implemented with the condition $y_0 = 1$ at a corresponding location x_0, and $y_m = 0$ at the endpoints. For one of the lines, we take $x_0 = -2/\sigma^2$, which corresponding to the virtual turning point. For all other lines, the value of x_0 is shifted from this point in a direction perpendicular to the lines x_m. Comparisons are made for several values of $\mathrm{Arg}(\sigma)$ with $\epsilon = 0.125$ and $|\sigma| = 1$, so that in each plot the solutions y_m have a different orientation.

This numerical setup does not correspond to the specific solution of section 3.2, which uses a different boundary condition as $|x_m| \to \infty$ in the complex plane; however, both solutions must exhibit the same Stokes structure. These simulations therefore provide a numerical validation of the Stokes structure predicted by the steepest descent analysis.

The Stokes structure predicted through asymptotic analysis matches the numerical results, showing oscillatory behavior with a slowly varying envelope between the turning points in the enclosed region $\mathcal{D}_3$, and exponential decay in the outer regions $\mathcal{D}_1$ and $\mathcal{D}_2$.

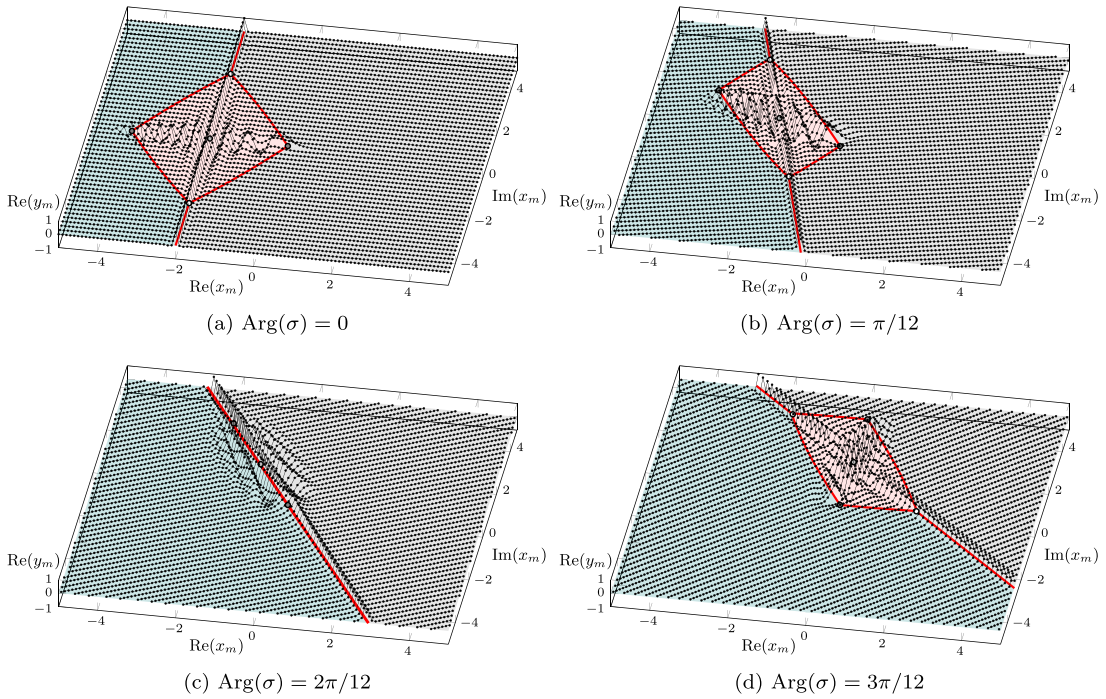

(a) $\mathrm{Arg}(\sigma) = 0$ (b) $\mathrm{Arg}(\sigma) = \pi/12$

(c) $\mathrm{Arg}(\sigma) = 2\pi/12$ (d) $\mathrm{Arg}(\sigma) = 3\pi/12$

Figure 12. Comparison of the Stokes structure (red) of our asymptotic solutions (20) to the advance-delay Airy equation (3) with numerical solutions of the discrete Airy equation (1) along several lines x_m throughout the complex plane, for several values of $\mathrm{Arg}(\sigma)$ with $\epsilon = 0.125$ and $|\sigma| = 1$. Numerical solutions (black), are normalized along each line x_m to have a maximum value of 1. The asymptotic and numerical results are in close agreement, showing oscillations with a slowly varying envelope in $\mathcal{D}_3$ and exponential decay in $\mathcal{D}_1$ and $\mathcal{D}_2$.

5. Discussion and conclusions

5.1. Explanation in terms of the Borel Plane

This study demonstrated that the HOSP appears in the asymptotic limit when a homogeneous linear second-order differential equation is discretized. By understanding the mechanism that causes this behavior to appear, we can argue that such behavior is, in fact, generic in linear discretized equations. Additionally, we will explain the impact of this effect on systems in which HOSP and Stokes curve accumulations already appear: nonlinear discrete equations.

The change in behavior that we see occurs because the continuous Airy equation possesses two exponential contributions (with exponents $\phi(x) = \pm 2x^{3/2}/3$, from (8)), while the discrete Airy equation possesses an infinite number of such exponential contributions ($\phi(x) = \phi_s^{\pm}$ from (15)). As a consequence, it is possible to have three or more exponentials interacting in a fashion that produces more complicated Stokes structures. While it is not apparent from the steepest descent analysis, the factorial-over-power analysis from appendix shows that in general we can expect an infinite number of exponential contributions to be present in discrete equations obtained by discretizing continuous systems.

In our problem, the singulant equation contained in (36) simplifies (for $\sigma = 1$) to give

$$\cosh\left(\frac{\mathrm{d}\phi}{\mathrm{d}x}\right) = 1 + \frac{x}{2}, \tag{22}$$

which must be satisfied by every choice of ϕ. Solving this equation generates an infinite number of values for $\mathrm{d}\phi/\mathrm{d}x$ that differ by $2\pi\mathrm{i}$ due to the Riemann sheet structure of the hyperbolic cosine function. This results in the asymptotic expansion containing an infinite number of exponential terms. These exponential terms group into two families, with the exponents

$$\phi_s^{\pm} = -\mathrm{i}\left[(x+2)\left(\pm\mathrm{i}\cosh^{-1}\left(1+\frac{x}{2}\right) - 2\pi s\right) \mp \mathrm{i}\sqrt{x(x+4)}\right]. \tag{23}$$

The two families are indexed by the sign choice. In this problem, the HOSP occurs due to interactions between exponents from the different families (see (18)–(19)). We will later explain why this must necessarily be the case.

The reason for the more complicated singulant expression in (22) is that the equation (3) contains terms that balance asymptotically with the discretized second derivative. However, the appearance of the

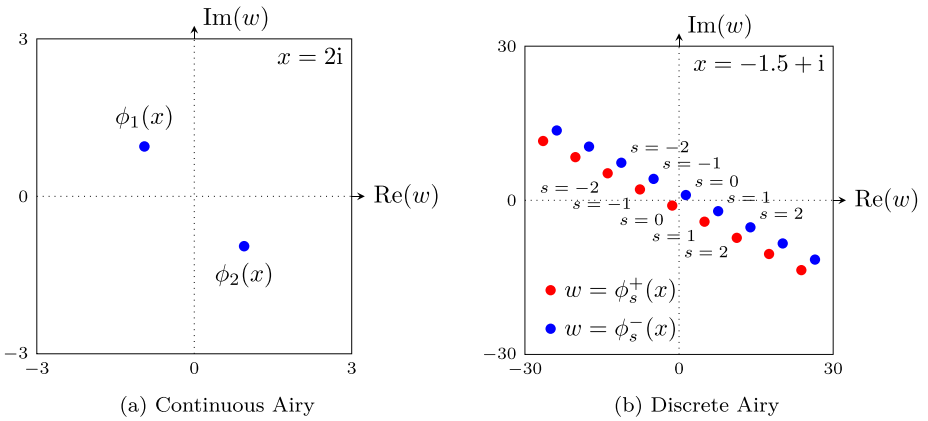

(a) Continuous Airy (b) Discrete Airy

Figure 13. Singularities in the Borel plane at particular values of x for (a) the continuous Airy equation (1) and (b) the advance-delay Airy equation (3). Figure (b) depicts two infinite lines of singularities emanating from $\phi_0^{\pm}$ respectively.

infinite number of exponentials is a consequence of how the discretized second derivative is treated by the late-order term analysis; hence, we expect this behavior to be generic in discretized second-order differential equations. Similar arguments can be made for infinite families of such terms to be generic for the discretization of higher-order derivatives.

A useful way to visualize exponential interactions is to study the asymptotic representation of the solution in the so-called *Borel plane*. The Borel-plane representation provides a useful framework for understanding how our results may be expected to generalize to discretizations of other linear and nonlinear equations. By taking the Borel transform in the fashion described in [3], effectively an inverse Laplace transform mapping x to a new variable w, we can identify key features of the asymptotic solution by examining the location of singular points in the transformed domain. The resultant transformed expression is singular at all points $w = \phi(x)$, and that these singularities move as x is varied.

An example schematic of singularity locations in the Borel plane for the solutions to the continuous and discrete Airy equations respectively is shown in figures 13(a) and (b). In figure 13(a) there are two singular points at $w = \phi_{1,2}(x)$, corresponding to the two exponential contributions to the Airy function asymptotics. In figure 13(b) there are an infinite number of singular points, located at $w = \phi_s^{\pm}(x)$, which divide into the expected two families (denoted by red and blue circles respectively).

Stokes switching can occur when the condition (4) is satisfied, which corresponds to the two singularities being on the same horizontal line in the Borel plane. This condition for Stokes switching occurs because the subdominant exponential (corresponding to the the leftmost singularity) is captured by the contour integral required to invert the Borel transform only when it crosses this horizontal line extending from the singularity associated with the dominant exponential. An example inversion contour with Stokes switching is shown in figure 14(a).

Furthermore, considering the Borel plane motivates the definition (6), which corresponds to three singularities being *colinear* in this plane. Stokes switching can only occur if the two singularities involved are on the same Riemann sheet (this is what it means for two contributions to be 'adjacent' when interpreted in terms of the Borel transform). Singularities can change between Riemann sheets across lines of co-linearity between three saddles, which produces the HOSC condition in (6). This brief explanation is sufficient to understand how the HOSP and Stokes curve accumulations arise; however, a more complete mathematical explanation may be found in [3]. An schematic of the HOSP in the Borel plane is shown to illustrate this idea in figure 14(b).

In the Borel plane, the singularities associated with exponentials introduced by equations such as (22) appear along *rays* in the Borel plane emanating from the singularity at $w = \phi_0^{\pm}(x)$. This is shown in figure 13(b). There are two singularity rays, associated with the two sign choices. As x varies, the distribution of singularities can rotate and scale in w, but they remain regularly spaced along the same ray.

The behavior of these rays explains the appearance of HOSC in figure 3. The values of x which correspond to the HOSC are when the rays in the Borel plane are aligned, allowing for the co-linearity condition (6) to be satisfied by a set of singularities that do not all lie on the same ray. This is shown in figure 15. Note that this condition can only be satisfied by all singularities on a ray at once, so we only see a single HOSC, despite the presence of an infinite number of singularities. A HOSP occurs between

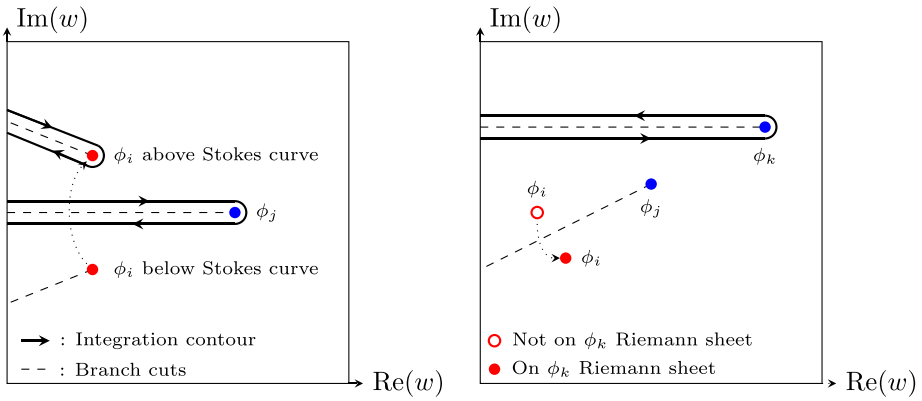

(a) Stokes switching (b) Higher-order Stokes switching

Figure 14. Schematics illustrating (a) the Stokes phenomenon described by (4), and (b) the higher-order Stokes phenomenon described by (6). In each case, the singularity that is switching is shown in red, and the dotted arrow shows its path as x is varied. In (a) the singularity contribution from ϕ_i is only picked up by the inversion integral contour when it crosses the horizontal line extending from ϕ_j, which is the Stokes curve represented in the Borel plane. In (b) the singularity contribution from ϕ_i lies on a different Riemann sheet to ϕ_k. When it crosses the branch cut associated with ϕ_j, it returns to the same Riemann sheet as ϕ_k and Stokes switching between the two is now possible; this means ϕ_i and ϕ_k are now adjacent.

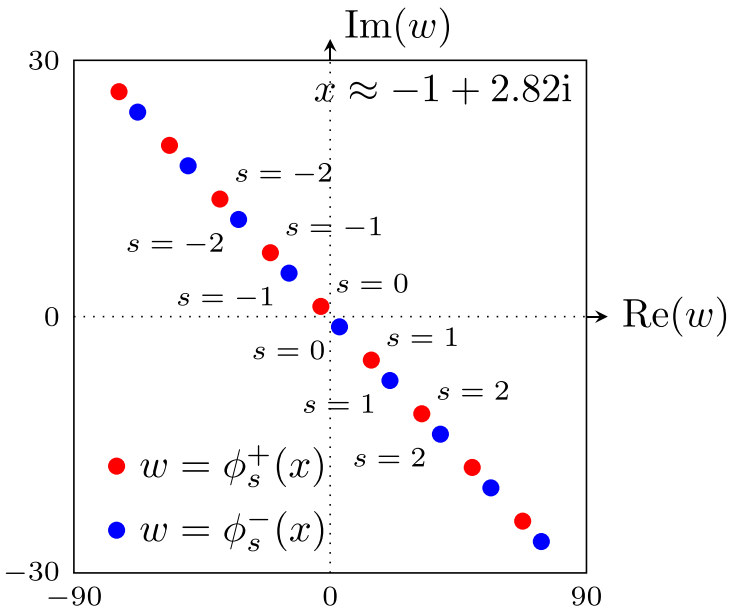

Figure 15. Singularities in the Borel plane where x is chosen to lie on the HOSC ($x \approx -1 + 2.82\mathrm{i}$). All singularities are co-linear, and a HOSP occurs between each group of three consecutive singularities. In each group of three, two from one exponent family are separated by one from the other.

each group of three consecutive singularities, which consists of two singularities from one family separated by one singularity from the other. This explains why the two relevant HOSC conditions in (6) contain either two contributions from ϕ_s^+ and one contribution from ϕ_s^- or vice versa.

The interaction of rays of singularities in the Borel plane also explains the accumulation of Stokes curves. In the discrete Airy equation, the Stokes curve condition (4) is satisfied by an infinite number of distinct exponent pairs (i.e. choices of ϕ_i and ϕ_j) on each Stokes curve in the accumulation. In each case, the exponent selected as ϕ_i and ϕ_j come from distinct exponential families, and the corresponding singularities in the Borel plane lie on different rays. This behavior is generic in any system that contains two (or more) rays of singularities in the Borel plane, corresponding to two (or more) families of exponential contributions. Consequently, this behavior can be expected to extend to any problem in which discretization produces two or more infinite families of exponentials.

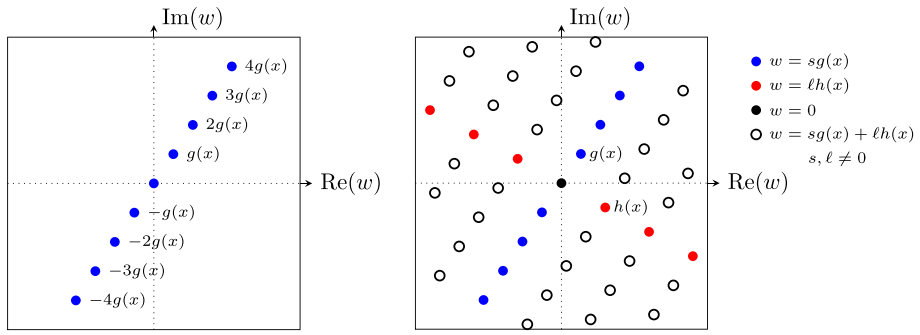

(a) Nonlinear with one exponential family (b) Nonlinear with two exponential families

Figure 16. Schematic of singularities in the Borel plane for continuous nonlinear problems with (a) one base exponential with $\phi = g(x)$, and (b) two base exponentials with $\phi = g(x)$ and $\phi = h(x)$. In (b) the resultant asymptotic expansion contains all exponentials of the form $\phi = sg(x) + \ell h(x)$ for $s, \ell \in \mathbb{Z}$.

5.1.1. Generalization to linear and nonlinear equations

It is straightforward to show that the discretization of derivatives will generally result in similar hyperbolic cosine and sine terms; these will have an infinite number of solutions when inverted, leading to an infinite family of exponential contributions. Results in previous studies suggest that such behavior is generic to discrete equations. For instance, any discretized second-order equation of the form

$$y(x+\epsilon) - 2y(x) + y(x-\epsilon) + f(x) = 0, \tag{24}$$

such as those of [50, 53]. By expanding the shifted terms around $\epsilon = 0$ and then applying late-order analysis in the manner introduced by [50], we see that equations of this form must generate exponentials with $\cosh(\mathrm{d}\phi/\mathrm{d}x) = 1$, and hence produce $\mathrm{d}\phi/\mathrm{d}x = 2\pi i s$ for $s \in \mathbb{Z}$. The reason for the more complicated expression in (22) is that the equation contains terms that balance asymptotically with the differential term, but the appearance of the infinite number of exponentials remains a consequence of how the discretized second derivative is treated by the late-order term analysis. Hence, we expect this behavior to be generic in discretized second-order differential equations.

As with the HOSP, we expect that this Stokes curve accumulations appear in general for systems that contain two (or more) families of exponential contributions, and hence two (or more) rays of singularities in the Borel plane, when discretized. This explains why such behavior is not present in the asymptotic solutions to equations of the form (24); in this case, discretization only introduces one infinite family of exponential contributions, rather than two.

While our analysis suggests that the appearance of the HOSP is generic in discretized linear differential equations with two or more exponentially families, we expect that more complicated behavior can arise in the study of discretized *nonlinear* differential equations, such as the discrete Painlevé equations [16].

In nonlinear equations, the general form of the transseries changes; if the singulant equation generates an exponential associated with some $\phi = g(x)$, then the effect of nonlinearity is to introduce exponentials of the form $\phi = sg(x)$ for all $s \in \mathbb{Z}$. This behavior is depicted in figure 16(a). Consequently, we expect that discretizing nonlinear equations will produce rays of singularities associated with nonlinear effects in addition to rays of singularities caused by the discretization.

This alone might suggest that the range of possible Stokes curve behaviors is similar to the linear problem, with two families of Borel plane singularities lying along rays, as in figure 13; however, there is a further additional effect seen in nonlinear equations which implies the presence of additional structure in the asymptotic solution. If a nonlinear equation contains multiple exponential contributions, say $g(x)$ and $h(x)$, then the asymptotic expression generally contains exponentials of the form $\phi(x) = sg(x) + \ell h(x)$ where $s, \ell \in \mathbb{Z}$. As a consequence, instead of having two distinct rays of singularities, the generic structure in the Borel plane can be expected to contain a *lattice* of singularities, such as that depicted in figure 16(b), rather than two just two distinct rays of singularities as in 13(b).

If we discretize a nonlinear differential equation, our results indicate that this will generally introduce new families of exponential contributions, and hence new rays of singularities in the Borel plane. Therefore, we conjecture that the presence of news ray due to discretization means that the expected structure of singularities in the Borel plane will not just be two interacting rays of singularities, but rather a lattice similar to figure 16(b). The only difference between thee two cases is that the family of

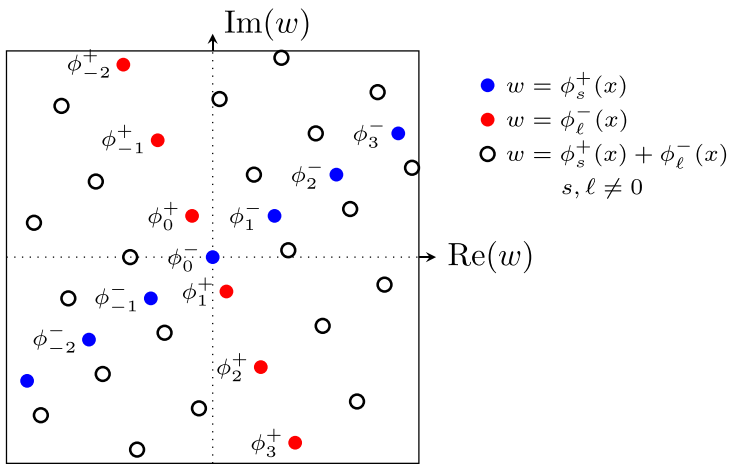

Figure 17. Singularity locations in the Borel plane for a discretized nonlinear equation with a family of exponentials with exponents $\phi = \phi^+_s(x)$ and $\phi = \phi^-_\ell(x)$ caused by discretization. This induces a Borel plane singularity lattice similar to figure 16(b), with an extra row due to the fact that $\phi^+_0(x)$ does not lie on the origin.

singularities associated with discretization may not necessarily have a singularity at $w = 0$, but might instead be offset, as seen in figure 13(b).

Consequently, if the asymptotic behavior of a nonlinear discretized problem contains, for example, two families of exponentials due to discretization: one with $\phi(x) = \phi^+_s(x)$ and one with $\phi(x) = \phi^-_\ell(x)$, then we expect that the resultant asymptotic expression to *also* contain all exponentials with form $\phi(x) = \phi^+_s(x) + \phi^-_\ell(x)$, where $s, \ell \in \mathbb{Z}$. An example of the Borel plane singularities associated with this structure is depicted in figure 17. This is very similar to the schematic in figure 16(b), with the only difference being that the two rays are no longer required to intersect at the origin. Note that even more complicated structures could emerge if a solution contains additional exponential families due to discretization or additional exponentials caused by nonlinear effects in the equation (as in figure 16(b)).

This Borel plane lattice structure permits a much richer variety of Stokes interactions caused by the many different Stokes, anti-Stokes and HOSCs that can occur due to the presence of a lattice of singularities. Hence any analysis of the Stokes phenomenon of discrete nonlinear equations must be approached carefully in order to keep track of all possible interactions. These observations may also have important consequences for rigorous analysis, and bounding of, the behavior of solutions of linear and nonlinear discrete equations, as they indicate that any rigorous analysis must take into account substantially more potential sources of exponential growth than the corresponding analysis for continuous linear differential equations.

5.2. Comparison with existing literature

In our study of the discrete Airy equation (2), we determined the transseries solution (20), whose coefficients vary across the regions $\mathcal{D}_1$, $\mathcal{D}_2$, and $\mathcal{D}_3$. These regions are bounded by active Stokes curves. The coefficient changes arise from the Stokes phenomenon as these Stokes curves are crossed. The Stokes curves originate at two turning points and a virtual turning point, and truncate at two SCPs. At the SCPs, HOSC emerge, across which the HOSP occurs, truncating the active Stokes curves.

A key novelty of our work is the identification of a virtual turning point at $x = -2/\sigma^2$ and the associated HOSP. These features were not observed in previous studies [17, 19, 23, 25–28, 35, 54], which focus on solutions along lines through the origin. Detecting the virtual turning point requires analytic continuation away from such lines, and hence the Stokes structure in the complex plane was not considered. Although [25] presents a related Stokes structure for a different discrete equation, the Stokes curves in that case do not intersect, and thus no virtual turning point or HOSP is observed.

The turning points at $x = -4/\sigma^2$ and $x = 0$, agree with those identified using direct series methods [17, 19, 26–28] and WKBJ methods [23, 25, 35, 54]. Near the turning points, the solution (20) follows an Airy function envelope, away from these points, the solution deviates from Airy function behavior, in agreement with these prior findings.

Near the turning points, the geometry of the active Stokes curves resembles that of the Airy function, consistent with studies [23, 25, 35, 55, 56]. Away from these points, the Stokes structure deviates due to differences in the singulants of the advance-delay Airy equation (3) and the continuous Airy equation (1). As previous studies consider different discrete equations, a direct comparison of the

Stokes structure is not possible, however, deviation from Airy function behavior is consistently observed [25, 35, 55, 56].

In section 3.4, we examine how the Stokes structure depends on both Argσ and $|\sigma|$ for complex step directions h. Previous studies [17, 19, 26–28] developed different asymptotic constructions based on relative positioning of the turning points, consistent with our observations of the Stokes structure as σ is varied.

5.3. Conclusions

In this work, we applied exponential asymptotic techniques to calculate asymptotic solutions to the discrete Airy equation (2). The resultant asymptotic expressions contain both the HOSP and Stokes curve accumulations; neither of these features occur for homogeneous linear second-order differential equations. In general, the HOSP requires at least three interacting exponential contributions, while Stokes curve accumulations require a transseries with an infinite number of exponential contributions. The process of discretization, even if it is linear, generates such a transseries solution and allows for the generation of effects that are restricted to higher-order or nonlinear homogeneous differential equations.

We showed that solutions to the discrete Airy equation (2) are described by the transseries (20). By comparing our solutions to the discrete Airy equation (2) with those of the continuous Airy equation (1), we found that discretization significantly alters both the asymptotic form and the associated Stokes structure. Specifically, solutions to the discrete Airy equation (2) have an additional turning point at $x=-4/\sigma^2$ and an additional virtual turning point at $x=-2/\sigma^2$, which generates new Stokes curves that intersect at two distinct SCPs. These features are absent in the continuous case.

We also identified the HOSP associated with the SCPs. Although the HOSP has been observed in the Gamma function $\Gamma(z)$, e.g. [38–40], to the authors' knowledge, the current analysis is the first observation and study of the HOSP in a discretization of a second order linear equation. In continuous equations, the HOSP emerges from the intersection of Stokes curves [2, 3]. Prior studies of other discrete equations [25] did not observe the HOSP, because they study different difference equations in which their corresponding Stokes curves did not intersect.

Because the asymptotic solution (20) is an infinite-parameter transseries with two distinct solution families, we observed accumulations of both an infinite number of Stokes and anti-Stokes curves. The accumulation of curves in the Stokes structure is often associated with nonlinear differential equations and is an expected consequence of nonlinearity as seen in [47]. Our results show that similar behavior can arise even in linear discrete systems with a finite number of turning points. This is a direct consequence of discretization, which necessarily introduces an infinite number of exponential contributions. We therefore conjecture that the accumulation of Stokes and anti-Stokes curves may be a generic feature of discrete equations, independent of nonlinearity.

Finally, we have also given indications of how the HOSP is likely to be generally widespread in discretizations of linear and nonlinear continuous systems, which has significant consequences for the complexity of carrying out a complete analysis of their asymptotic behaviors.

Data availability statement

No new data were created or analysed in this study.

Acknowledgments

The authors would like to thank the Isaac Newton Institute for Mathematical Sciences, Cambridge, for support and hospitality during the program 'Applicable resurgent asymptotics: towards a universal theory', where the work on this paper was conceptualized. The program was supported by the EPSRC Grant No. EP/R014604/1. We thank the anonymous reviewers for suggestions that substantially improved the quality of the manuscript.

Funding

AJMD and CJL gratefully acknowledge funding from ARC Discovery Project DP190101190. CJL gratefully acknowledges funding from ARC Discovery Project DP240101666.

Author contributions

Aaron J Moston-Duggan 0000-0003-1189-4065
Conceptualization (equal), Formal analysis (equal), Visualization (equal), Writing – original draft (equal), Writing – review & editing (equal)

Christopher J Howls 0000-0001-7989-7807
Writing – original draft (equal), Writing – review & editing (equal)

Christopher J Lustri 0000-0001-9504-277X
Conceptualization (equal), Supervision (equal), Writing – review & editing (equal)

Appendix. Factorial-over-power analysis

In this section, we show that the asymptotic solution (20) to the discrete Airy equation (2), previously derived by steepest descent, can also be obtained using exponential asymptotics based on factorial-over-power methods [15, 51]. Unlike steepest descent, this approach does not require an integral representation and applies directly to the advance-delay equation (3). Demonstrating this method is valuable, as it extends naturally to nonlinear problems and provides a useful tool for studying the HOSP in nonlinear difference equations.

To apply the factorial-over-power methods, we expand the solution to (3) as a Taylor series about $\epsilon = 0$ and obtain

$$\frac{2}{\sigma^2}\sum_{j=1}^{\infty}\frac{\sigma^{2j}\epsilon^{2j}}{(2j)!}\frac{\mathrm{d}^{2j}y}{\mathrm{d}x^{2j}} - xy = 0\,, \tag{25}$$

where $y(x)$ is now a local expression. We study equation (25) using exponential asymptotic methods developed in [15] and first applied to discrete systems in [50].

A.1. Methodology

The steepest descent method is effective for deriving asymptotic solutions from integrals, however, many problems lack a convenient integral form. In such cases, exponential asymptotic methods [15, 51] can be applied directly to the differential equation to determine the same asymptotic results as the steepest descent analysis.

We first expand the solution as an asymptotic power series of the form

$$y \sim \left(\sum_{k=0}^{\infty}\epsilon^k A_k(x)\right)\mathrm{e}^{-\phi(x)/\epsilon} \qquad \text{as} \qquad \epsilon \to 0\,. \tag{26}$$

We substitute the asymptotic series (26) into the governing equation and match the terms for all orders of ϵ. Solving these equations for each order of ϵ gives the values of ϕ and A_k.

Determining A_k requires repeated differentiation of earlier terms. When these terms are singular, this causes 'factorial-over-power' divergence [14], enabling an asymptotic description of the late-order terms A_k as $k \to \infty$. Based on [14], the authors of [15] proposed an ansatz for late-order terms, the leading-order term is a sum of terms of the form

$$A_k \sim \frac{B(x)\,\Gamma(k+\gamma)}{\chi(x)^{k+\gamma}} \qquad \text{as} \qquad k \to \infty\,, \tag{27}$$

where Γ is the gamma function, γ is a constant and B and χ are functions of x. Each term in the sum is associated with a particular singularity of A_0. The contribution for each singularity can be determined independently, taking the sum of these contributions provides the complete behavior of the late-order terms [14].

We call the functions B the prefactor and χ the singulant. The singulants satisfy $\chi = 0$ at the singularities of A_0, ensuring that A_k is also singular at the same location. Substituting the ansatz (27) into the recurrence relation and matching terms as $k \to \infty$ determines B and χ. The value of γ is chosen to ensure consistency of late-order terms (27) with the leading-order solution A_0 near the singularities.

The singulant χ determines the location of Stokes curves. As shown by [14], a Stokes curve associated with a change in exponentially small behavior that is switched by a power series expansion, satisfies the conditions

$$\mathrm{Im}(\chi) = 0 \quad \text{and} \quad \mathrm{Re}(\chi) > 0\,. \tag{28}$$

The first condition ensures the dominant and subdominant exponential contributions have equal phase, while the second restricts Stokes switching to exponentially small contributions. We note that in this formulation the singulant $\chi = \phi_1 - \phi_2$ is the difference between the exponents of two distinct exponential contributions, and therefore condition (28) is equivalent to condition (4).

Knowing the late-order form (27) allows optimal truncation of the divergent series (26) at the smallest term, typically producing an exponentially small error as $\epsilon \to 0$ [57–59]. The optimally truncated series is given as

$$y = \left(\sum_{k=0}^{K-1} \epsilon^k A_k + R_K \right) \mathrm{e}^{-\phi/\epsilon} \quad \text{as} \quad \epsilon \to 0\,, \tag{29}$$

where the remainder R_K is exponentially small as $\epsilon \to 0$. The optimal truncation point K occurs at the term of least magnitude [59]. Applying this heuristic to (27) gives $K \sim |\chi|/\epsilon$.

We determine the exponentially small remainder R_K by substituting (29) into the original equation. Away from the Stokes curves, we approximate R_K using the WKBJ ansatz [13]. The WKBJ approximation breaks down near the Stokes curve. Near the Stokes curve, we determine R_K using the variation of parameters ansatz

$$R_K \sim \mathcal{M}(x)\, B(x)\, \mathrm{e}^{-\chi(x)/\epsilon} \quad \text{as} \quad \epsilon \to 0\,, \tag{30}$$

where $\mathcal{M}$, is called the Stokes multiplier, which varies rapidly in a width of $\mathcal{O}(\epsilon^{1/2})$ around the Stokes curve and encodes the Stokes switching. We compute $\mathcal{M}$ using the matched asymptotic expansion procedure from [51].

A.2. Series expansion

Substituting the ansatz (26) into (25) to obtain

$$\frac{2}{\sigma^2} \sum_{j=1}^{\infty} \sum_{k=0}^{\infty} \frac{\sigma^{2j} \epsilon^{2j+k}}{(2j)!} \frac{\mathrm{d}^{2j}}{\mathrm{d}x^{2j}} \left(A_k \mathrm{e}^{-\phi/\epsilon} \right) - x \sum_{k=0}^{\infty} \epsilon^k A_k \mathrm{e}^{-\phi/\epsilon} = 0\,. \tag{31}$$

We apply the general Leibniz rule and Faá di Bruno's formula to write

$$\frac{\mathrm{d}^{2j}}{\mathrm{d}x^{2j}} \left(A_k \mathrm{e}^{-\phi/\epsilon} \right) = \sum_{l=0}^{2j} \frac{(2j)!}{l!\,(2j-l)!} \frac{\mathrm{d}^{2j-l} A_k}{\mathrm{d}x^{2j-l}} \sum_{m=0}^{l} \frac{(-1)^m \mathcal{B}^{\phi}_{l,m}}{\epsilon^m} \mathrm{e}^{-\phi/\epsilon}\,, \tag{32}$$

where $\mathcal{B}^{\phi}_{l,m}$ are the partial Bell polynomials [60] where the superscript notation indicates the argument, such that

$$\mathcal{B}^{\phi}_{l,m} = \mathcal{B}_{l,m} \left(\frac{\mathrm{d}\phi}{\mathrm{d}x}, \frac{\mathrm{d}^2\phi}{\mathrm{d}x^2}, \cdots, \frac{\mathrm{d}^{l-m+1}\phi}{\mathrm{d}x^{l-m+1}} \right). \tag{33}$$

The partial Bell polynomials allow our expressions to be written compactly. We will make use of the identities

$$\mathcal{B}^{\phi}_{l,l} = \left(\frac{\mathrm{d}\phi}{\mathrm{d}x} \right)^l \quad \text{and} \quad \mathcal{B}^{\phi}_{l,l-1} = \binom{l}{2} \left(\frac{\mathrm{d}\phi}{\mathrm{d}x} \right)^{l-2} \frac{\mathrm{d}^2\phi}{\mathrm{d}x^2}\,. \tag{34}$$

We apply (32) to (31) to obtain

$$\frac{2}{\sigma^2} \sum_{j=1}^{\infty} \sum_{k=0}^{\infty} \sum_{l=0}^{2j} \sum_{m=0}^{l} \frac{(-1)^m \sigma^{2j} \epsilon^{2j+k-m} \mathcal{B}^{\phi}_{l,m}}{l!\,(2j-l)!} \frac{\mathrm{d}^{2j-l} A_k}{\mathrm{d}x^{2j-l}} - x \sum_{k=0}^{\infty} \epsilon^k A_k = 0\,. \tag{35}$$

A.2.1. Exponent equation

We balance the terms in (35) at $\mathcal{O}(1)$ as $\epsilon \to 0$. After using the identities from (34), we obtain

$$0 = \frac{2}{\sigma^2} \sum_{j=1}^{\infty} \frac{\sigma^{2j}}{(2j)!} \left(\frac{\mathrm{d}\phi}{\mathrm{d}x} \right)^{2j} - x = \frac{2}{\sigma^2} \left(\cosh\left(\sigma \frac{\mathrm{d}\phi}{\mathrm{d}x} \right) - 1 \right) - x\,. \tag{36}$$

Solving this equation gives two families of solutions for ϕ

$$\phi_s^{\pm} = -\frac{\mathrm{i}}{\sigma}\left[\left(x+\frac{2}{\sigma^2}\right)\left(\pm \mathrm{i}\cosh^{-1}\left(1+\frac{\sigma^2 x}{2}\right)-2\pi s\right)\mp \mathrm{i}\sqrt{x(\sigma^2 x+4)}\right]. \tag{37}$$

We label the families by a superscript for the sign choice and a subscript for the index s. The exponents $\phi_s^{\pm}$ (37) correspond to the saddle heights (15) from the steepest descents analysis. The solution then takes the form

$$y \sim \sum_{s=-\infty}^{\infty}\left[c_s^{+}\sum_{k=0}^{\infty}\epsilon^k A_{s,k}^{+}\mathrm{e}^{\phi_s^{+}/\epsilon}+c_s^{-}\sum_{k=0}^{\infty}\epsilon^k A_{s,k}^{-}\mathrm{e}^{\phi_s^{-}/\epsilon}\right] \quad \text{as} \quad \epsilon\to 0, \tag{38}$$

where $c_s^{\pm}$ are constants to be specified in one of the regions $\mathcal{D}_1$, $\mathcal{D}_2$, or $\mathcal{D}_3$ to obtain a particular solution to (3).

A.2.2. Leading-order solution

We continue to balance terms in equation (35) of size $\mathcal{O}(\epsilon)$ as $\epsilon\to 0$ in order to determine the form of the leading-order terms in (38), $A_{s,0}^{\pm}$. Simplifying the resultant expression using (34) and (36) gives

$$0 = \sum_{j=1}^{\infty}\frac{\sigma^{2j}}{(2j-1)!}\left(\frac{\mathrm{d}\phi_s^{\pm}}{\mathrm{d}x}\right)^{2j-1}\frac{\mathrm{d}A_{s,0}^{\pm}}{\mathrm{d}x}+\frac{\mathrm{d}^2\phi_s^{\pm}}{\mathrm{d}x^2}\sum_{j=1}^{\infty}\frac{\sigma^{2j}}{2!\,(2j-2)!}\left(\frac{\mathrm{d}\phi_s^{\pm}}{\mathrm{d}x}\right)^{2j-2}A_{s,0}^{\pm} \tag{39}$$

$$= \sinh\left(\sigma\frac{\mathrm{d}\phi_s^{\pm}}{\mathrm{d}x}\right)\frac{\mathrm{d}A_{s,0}^{\pm}}{\mathrm{d}x}+\frac{\sigma}{2}\cosh\left(\sigma\frac{\mathrm{d}\phi_s^{\pm}}{\mathrm{d}x}\right)\frac{\mathrm{d}^2\phi_s^{\pm}}{\mathrm{d}x^2}A_{s,0}^{\pm}. \tag{40}$$

We solve equation (40) to obtain

$$A_{s,0}^{\pm} = \frac{1}{\sqrt{2\pi\epsilon}x^{1/4}\left(\sigma^2 x+4\right)^{1/4}}, \tag{41}$$

where the multiplicative constants are included for later algebraic convenience.

The leading-order behavior of each exponential contribution as $\epsilon\to 0$ is therefore given by

$$y_{s,0}^{\pm} = \frac{1}{\sqrt{2\pi\epsilon}x^{1/4}\left(\sigma^2 x+4\right)^{1/4}}\mathrm{e}^{\left(\frac{\mathrm{i}}{\sigma\epsilon}\left[\left(x+\frac{2}{\sigma^2}\right)\left(\pm\mathrm{i}\cosh^{-1}\left(1+\frac{\sigma^2 x}{2}\right)+2\pi s\right)\mp\mathrm{i}\sqrt{x(\sigma^2 x+4)}\right]\right)}. \tag{42}$$

Each contribution has two singularities, giving the turning points $x=-4/\sigma^2$ and $x=0$, in agreement with those identified from the steepest descent analysis.

A.3. Late-order terms

To calculate all series terms $A_{s,k}^{\pm}$, we match the terms in (35) at each power of ϵ and solve each equation recursively. Since the analysis applies identically to all $\phi_s^{\pm}$, we simplify the notation by writing $\phi_s^{\pm}=\phi$ and $A_{s,k}^{\pm}=A_k$.

Balancing terms in (35) at order $\mathcal{O}(\epsilon^q)$ with $q\geqslant 2$ as $\epsilon\to 0$ gives

$$\frac{2}{\sigma^2}\sum_{j=\lfloor\frac{q-1}{2}\rfloor+1}^{\infty}\sum_{m=2j-q}^{2j}\sum_{l=m}^{2j}\frac{(-1)^m\sigma^{2j}\mathcal{B}_{l,m}^{\phi}}{l!\,(2j-l)!}\frac{\mathrm{d}^{2j-l}A_{m+q-2j}}{\mathrm{d}x^{2j-l}}$$

$$+\frac{2}{\sigma^2}\sum_{j=1}^{\lfloor\frac{q-1}{2}\rfloor}\sum_{m=0}^{2j}\sum_{l=m}^{2j}\frac{(-1)^m\sigma^{2j}\mathcal{B}_{l,m}^{\phi}}{l!\,(2j-l)!}\frac{\mathrm{d}^{2j-l}A_{m+q-2j}}{\mathrm{d}x^{2j-l}}-xA_q=0, \tag{43}$$

where $\lfloor\cdot\rfloor$ denotes the floor function. Each contribution $y_{s,0}^{\pm}$ (42) is singular at $x=-4/\sigma^2$ and $x=0$, so the asymptotic series (26) exhibit factorial-over-power divergence. Hence, the terms A_k are described by

the late-order ansatz (27). We apply (27) to the recurrence relation (43) to obtain

$$\frac{2}{\sigma^2}\sum_{j=\lfloor\frac{q-1}{2}\rfloor+1}^{\infty}\sum_{m=2j-q}^{2j}\sum_{l=m}^{2j}\sum_{n=0}^{2j-l}\sum_{p=0}^{n}\frac{\Gamma(m+q+p+\gamma-2j)}{\chi^{m+q+p+\gamma-2j}}\frac{(-1)^{m+p}\sigma^{2j}\mathcal{B}^{\phi}_{l,m}\mathcal{B}^{\chi}_{n,p}}{l!n!(2j-l-n)!}\frac{\mathrm{d}^{2j-l-n}B}{\mathrm{d}x^{2j-l-n}}$$
$$+\frac{2}{\sigma^2}\sum_{j=1}^{\lfloor\frac{q-1}{2}\rfloor}\sum_{m=0}^{2j}\sum_{l=m}^{2j}\sum_{n=0}^{2j-l}\sum_{p=0}^{n}\frac{\Gamma(m+q+p+\gamma-2j)}{\chi^{m+q+p+\gamma-2j}}\frac{(-1)^{m+p}\sigma^{2j}\mathcal{B}^{\phi}_{l,m}\mathcal{B}^{\chi}_{n,p}}{l!n!(2j-l-n)!}\frac{\mathrm{d}^{2j-l-n}B}{\mathrm{d}x^{2j-l-n}}$$
$$-xB\frac{\Gamma(q+\gamma)}{\chi^{q+\gamma}}=0. \tag{44}$$

As $q\to\infty$, the first term will not contribute in any subsequent analysis and is henceforth neglected.

A.3.1. Singulant equation

We balance the largest terms in equation (44), which are of order $\mathcal{O}(A_q)$ as $q\to\infty$ to obtain

$$\frac{2}{\sigma^2}\sum_{j=1}^{\lfloor\frac{q-1}{2}\rfloor}\sum_{m=0}^{2j}\frac{\sigma^{2j}}{m!(2j-m)!}\left(\frac{\mathrm{d}\phi}{\mathrm{d}x}\right)^m\left(\frac{\mathrm{d}\chi}{\mathrm{d}x}\right)^{2j-m}-x=0. \tag{45}$$

We are considering the behavior of late-order terms (27), and therefore the large-q limit of (45). Extending the sums to infinity yields the leading-order behavior of (45) as $q\to\infty$, which gives

$$0=\frac{2}{\sigma^2}\sum_{j=1}^{\infty}\sum_{m=0}^{2j}\frac{\sigma^{2j}}{m!(2j-m)!}\left(\frac{\mathrm{d}\phi}{\mathrm{d}x}\right)^m\left(\frac{\mathrm{d}\chi}{\mathrm{d}x}\right)^{2j-m}-x \tag{46}$$
$$=\frac{2}{\sigma^2}\left(\cosh\left(\sigma\left(\frac{\mathrm{d}\phi}{\mathrm{d}x}+\frac{\mathrm{d}\chi}{\mathrm{d}x}\right)\right)-1\right)-x. \tag{47}$$

Solving (46) for $\mathrm{d}\chi/\mathrm{d}x$ we find two singulants for each exponent ϕ_s^- and ϕ_s^+. We denote these singulants as

$$\frac{\mathrm{d}\chi^{\pm,\pm}_{s,p}}{\mathrm{d}x}=\frac{2\pi\mathrm{i}(s-p)}{\sigma},\qquad \frac{\mathrm{d}\chi^{\pm,\mp}_{s,p}}{\mathrm{d}x}=\frac{2}{\sigma}\left(\pi\mathrm{i}(s-p)\pm\cosh^{-1}\left(1+\frac{\sigma^2x}{2}\right)\right), \tag{48}$$

where upper and lower sign choices correspond. The singulants $\chi^{-,-}_{s,p}$, $\chi^{-,+}_{s,p}$, $\chi^{+,-}_{s,p}$,and $\chi^{+,+}_{s,p}$ correspond to the Stokes switching behavior across the Stokes curves $\mathcal{S}^{-,-}_{s,p}$, $\mathcal{S}^{-,+}_{s,p}$, $\mathcal{S}^{+,-}_{s,p}$, and $\mathcal{S}^{+,+}_{s,p}$ respectively. The first superscript and subscript indicates the dominant exponential contribution, while the second indicates the exponential term that is switched on. For example, the singulant $\chi^{+,-}_{s,p}$ is associated with the y_s^+ contribution switching on the y_p^- contribution.

Although the series analysis can identify active Stokes curves, care is needed due to the many possible interacting contributions. To streamline the analysis, we instead use the steepest descent results to focus only on those Stokes curves known to be active in the asymptotic solution.

The Stokes curves $\mathcal{S}^{-,+}_{s,s}$ originate at the turning point $x=0$. Solving (48) with the condition $\chi=0$ at $x=0$ shows that the corresponding singulants are

$$\chi^{+,-}_{s,s}=\frac{2\mathrm{i}}{\sigma}\left[\left(x+\frac{2}{\sigma^2}\right)\mathrm{i}\cosh^{-1}\left(1+\frac{\sigma^2x}{2}\right)-\mathrm{i}\sqrt{x(\sigma^2x+4)}\right]. \tag{49}$$

The Stokes curves $\mathcal{S}^{-,+}_{s,s+1}$ originate at the turning point $x=-4/\sigma^2$. Solving (48) with the condition $\chi=0$ at $x=-4/\sigma^2$ shows that the corresponding singulants are

$$\chi^{-,+}_{s,s+1}=-\frac{2\mathrm{i}}{\sigma}\left[\left(x+\frac{2}{\sigma^2}\right)\left(\mathrm{i}\cosh^{-1}\left(1+\frac{\sigma^2x}{2}\right)+2\pi\right)-\mathrm{i}\sqrt{x(\sigma^2x+4)}\right]. \tag{50}$$

The Stokes curves $\mathcal{S}^{-,-}_{s,s+1}$ and $\mathcal{S}^{+,+}_{s,s+1}$ originate at the virtual turning point $x=-2/\sigma$. Solving (48) with $\chi=0$ at $x=-2/\sigma^2$ shows that the corresponding singulants are

$$\chi^{-,-}_{s,s+1} = \chi^{+,+}_{s,s+1} = \frac{2\pi \mathrm{i}}{\sigma}\left(x + \frac{2}{\sigma^2}\right). \tag{51}$$

Each singulant can be directly related to the corresponding steepest descent expression by noting that $\chi^{+,-}_{s,p} = \phi^+_s - \phi^-_p$, with the other singulants obtained by adjusting signs and indices accordingly. Applying condition (28) to each singulant yields the same Stokes curves as those found using the steepest descent method in section 3.

A.3.2. Prefactor equation

We balance the next to largest terms in equation (44), which are of order $\mathcal{O}(A_{q-1})$ as $q \to \infty$ to obtain

$$\frac{2}{\sigma^2}\sum_{j=1}^{\lfloor \frac{q-1}{2} \rfloor}\sum_{m=0}^{2j-1}\sum_{l=m}^{m+1}\sum_{n=2j-m-1}^{2j-l}\frac{\sigma^{2j}\mathcal{B}^{\phi}_{l,m}\mathcal{B}^{\chi}_{n,2j-m-1}}{l!n!\,(2j-l-n)!}\frac{\mathrm{d}^{2j-l-n}B}{\mathrm{d}x^{2j-l-n}} = 0. \tag{52}$$

We take the limit $q \to \infty$ in equation (52) and apply the identities from (34), to obtain

$$\sinh\left(\sigma\left(\frac{\mathrm{d}\phi}{\mathrm{d}x} + \frac{\mathrm{d}\chi}{\mathrm{d}x}\right)\right)\frac{\mathrm{d}B}{\mathrm{d}x} + \frac{\sigma}{2}\left(\frac{\mathrm{d}^2\phi}{\mathrm{d}x^2} + \frac{\mathrm{d}^2\chi}{\mathrm{d}x^2}\right)\cosh\left(\sigma\left(\frac{\mathrm{d}\phi}{\mathrm{d}x} + \frac{\mathrm{d}\chi}{\mathrm{d}x}\right)\right)B = 0. \tag{53}$$

We solve the prefactor equation (53) for each of the singulants, giving

$$B^{\pm}_s = \frac{C^{\pm}_s}{\sqrt{2\pi\epsilon}x^{1/4}\left(\sigma^2 x + 4\right)^{1/4}}. \tag{54}$$

where $C^{\pm}_s$ are constants that remain to be determined. The multiplicative constants in (54) are chosen for algebraic convenience, such that $C^{\pm}_s = 1$ in the final asymptotic expression.

Calculating C^+_s, C^-_s and γ: To determine C^+_s, we match the late-order ansatz (27) with a local expansion of the solution near the singularity $x = 0$. This is necessary because the outer expansion (26) of the late-order terms (27) breaks down in the region where $\epsilon^k A_k \mathrm{e}^{-\phi/\epsilon} \sim \epsilon^{k+1}A_{k+1}\mathrm{e}^{-\phi/\epsilon}$; that is, where $\chi = \mathcal{O}(\epsilon)$ as $k \to \infty$.

The singulant and the leading-order contribution satisfy

$$\chi^{+,-}_{s,s} \sim \frac{4x^{3/2}}{3} \qquad \text{and} \qquad A_0\mathrm{e}^{-S^+_s} \sim \frac{C^+_s}{2\sqrt{\pi\epsilon}x^{1/4}}\mathrm{e}^{\frac{2\mathrm{i}\pi}{\sigma}\left(x+\frac{2}{\sigma^2}\right)-\frac{2}{3}x^{3/2}} \qquad \text{as} \qquad x \to 0. \tag{55}$$

The envelope for the leading-order contribution and the singulant match those of the singularly-perturbed Airy equation (1). Furthermore, applying the inner scaling $x = \epsilon^{2/3}\eta$ and $\psi(\eta) = \epsilon^{-1/6}y(x)$, shows that the local equation for the discrete Airy equation (25) is the same as that of the continuous Airy equation (1).

The analysis therefore proceeds identically to that of the well-known Airy equation (1). For brevity, we omit repeating this analysis, and use the result that $C^+_s = 1$. A similar analysis shows $C^-_s = 1$.

The strength of the singularity in the late-order terms (27) must be consistent with the leading-order solutions (42) near the singularities $x = 0$ and $x = -4/\sigma^2$. The leading-order solution (42) has singularities of order 1/4 at these points. Since B is also singular with order 1/4, the late-order terms (27) are consistent with the leading-order solutions (42) if and only if $\gamma = 0$.

A.4. Stokes switching

We apply the exponential asymptotic method developed in [51], optimally truncating the divergent series (26) after K terms, yields the expression (29), where R_K denotes the remainder. Following the heuristic of [14, 59], the optimal truncation point is the value of K for which consecutive terms in the series have the same magnitude in the limit $\epsilon \to 0$. This typically occurs after an asymptotically large number of terms, so we use the late-order ansatz (27) to estimate K. The optimal truncation point satisfies $K \sim |\chi|/\epsilon$ as $\epsilon \to 0$, which justifies the use of the late-order ansatz. We therefore set $K = |\chi|/\epsilon + \omega$, where $\omega \in [0, 1)$ is chosen to ensure that K is an integer.

This follows directly from the method in [51]; however, it is not obvious that the governing equation (3) reduces to the standard form seen in exponential asymptotics. We therefore outline the details here. The analysis is presented for general χ and B, so it applies uniformly to each switching contribution in the solution.

We substitute the optimally truncated series (29) into (3) to obtain

$$\frac{2}{\sigma^2}\sum_{j=1}^{\infty}\sum_{l=0}^{2j}\sum_{m=0}^{l}\frac{(-1)^m\sigma^{2j}\epsilon^{2j-m}\mathcal{B}^{\phi}_{l,m}}{l!\,(2j-l)!}\frac{\mathrm{d}^{2j-l}R}{\mathrm{d}x^{2j-l}}-xR= \\ -\left(\frac{2}{\sigma^2}\sum_{j=1}^{\infty}\sum_{k=0}^{K-1}\sum_{l=0}^{2j}\sum_{m=0}^{l}\frac{(-1)^m\sigma^{2j}\epsilon^{2j+k-m}\mathcal{B}^{\phi}_{l,m}}{l!\,(2j-l)!}\frac{\mathrm{d}^{2j-l}A_k}{\mathrm{d}x^{2j-l}}-x\sum_{k=0}^{K-1}\epsilon^k A_k\right). \tag{56}$$

Simplifying (56) using (36), (40), and the recurrence relation (43), as $\epsilon\to 0$ we obtain the leading-order terms

$$\frac{2}{\sigma^2}\sum_{j=1}^{\infty}\sum_{l=0}^{2j}\sum_{m=0}^{l}\frac{(-1)^m\sigma^{2j}\epsilon^{2j-m}\mathcal{B}^{\phi}_{l,m}}{l!\,(2j-l)!}\frac{\mathrm{d}^{2j-l}R}{\mathrm{d}x^{2j-l}}-xR\sim-\frac{2\epsilon^{K+1}}{\sigma^2}\sum_{j=1}^{\infty}\sum_{l=2j-1}^{2j}\frac{\sigma^{2j}\mathcal{B}^{\phi}_{l,2j-1}}{l!\,(2j-l)!}\frac{\mathrm{d}^{2j-l}A_K}{\mathrm{d}x^{2j-l}}, \tag{57}$$

where the terms omitted in (57) are at most $\mathcal{O}(\epsilon^{K+2})$ as $\epsilon\to 0$ and are therefore negligible.

Since $K\to\infty$ as $\epsilon\to 0$, we insert the late-order ansatz (27) into (57) and retaining only the largest terms as $\epsilon\to 0$, we obtain in this limit

$$\frac{2}{\sigma^2}\sum_{j=1}^{\infty}\sum_{l=0}^{2j}\sum_{m=0}^{l}\frac{(-1)^m\sigma^{2j}\epsilon^{2j-m}\mathcal{B}^{\phi}_{l,m}}{l!\,(2j-l)!}\frac{\mathrm{d}^{2j-l}R}{\mathrm{d}x^{2j-l}}-xR\sim\frac{2\epsilon^{K+1}}{\sigma}\sinh\left(\sigma\frac{\mathrm{d}\phi}{\mathrm{d}x}\right)\frac{\mathrm{d}\chi}{\mathrm{d}x}\frac{B\Gamma(K+1)}{\chi^{K+1}}, \tag{58}$$

where terms omitted from (58) have a size of at most $\mathcal{O}(\Gamma(K)/\chi^K)$ as $K\to\infty$ and are negligible in this analysis.

The right-hand side of (58) is small compared to the terms on the left-hand side, except within a region of width $\mathcal{O}(\sqrt{\epsilon})$ around the curve $\mathrm{Im}(\chi)=0$, which is the Stokes curve. Away from the Stokes curve, we use a WKBJ ansatz to solve the homogeneous version of (58), given by

$$\frac{2}{\sigma^2}\sum_{j=1}^{\infty}\sum_{l=0}^{2j}\sum_{m=0}^{l}\frac{(-1)^m\sigma^{2j}\epsilon^{2j-m}\mathcal{B}^{\phi}_{l,m}}{l!\,(2j-l)!}\frac{\mathrm{d}^{2j-l}R_K}{\mathrm{d}x^{2j-l}}-xR_K=0. \tag{59}$$

The WKBJ analysis of (59) motivates a variation of parameters approach using the ansatz (30) to describe the behavior of R_K near the Stokes curve. The Stokes multiplier $\mathcal{M}$ varies locally around the Stokes curve, where the right-hand side of (58) is not negligible, capturing the switching behavior. Substituting the ansatz (30) into (58), and simplifying using (36), (46), and (54), gives the Stokes multiplier equation

$$\frac{\mathrm{d}\mathcal{M}}{\mathrm{d}x}\sim-\frac{\sinh\left(\sigma\frac{\mathrm{d}\phi}{\mathrm{d}x}\right)\frac{\mathrm{d}\chi}{\mathrm{d}x}}{\sinh\left(\sigma\left(\frac{\mathrm{d}\phi}{\mathrm{d}x}+\frac{\mathrm{d}\chi}{\mathrm{d}x}\right)\right)}\frac{\epsilon^K\Gamma(K+1)}{\chi^{K+1}}\mathrm{e}^{\chi/\epsilon}\quad\text{as}\quad\epsilon\to 0. \tag{60}$$

The right-hand side of (60) simplifies since the first term is either 1 or -1, depending on χ, hence, we write

$$\frac{\mathrm{d}\mathcal{M}}{\mathrm{d}x}\sim\mp\frac{\mathrm{d}\chi}{\mathrm{d}x}\frac{\epsilon^K\Gamma(K+1)}{\chi^{K+1}}\mathrm{e}^{\chi/\epsilon}\quad\text{as}\quad\epsilon\to 0. \tag{61}$$

It is useful to make χ the independent variable. Applying this change of variables to (60) gives

$$\frac{\mathrm{d}\mathcal{M}}{\mathrm{d}\chi}\sim\mp\frac{\epsilon^K\Gamma(K+1)}{\chi^{K+1}}\mathrm{e}^{\chi/\epsilon}\quad\text{as}\quad\epsilon\to 0. \tag{62}$$

From this point, the analysis follows the standard matched asymptotic expansion method from [51], which gives

$$\mathcal{M}\sim\pm\mathrm{i}\pi\,\mathrm{erf}\left(\sqrt{\frac{|\chi|}{\epsilon}}\mathrm{Arg}(\chi)\right)+C\quad\text{as}\quad\epsilon\to 0, \tag{63}$$

where 'Arg' denotes the principal argument. This is the standard form of Stokes switching encountered in steepest descents analysis, confirming agreement with the results of section 3. Hence, the asymptotic behavior of the solution to the discrete Airy equation (2) can be determined using only asymptotic series methods.

References

[1] Stokes G G 1864 On the discontinuity of arbitrary constants which appear in divergent developments *Trans. Camb. Phil. Soc.* **10** 105
[2] Chapman S J and Mortimer D B 2005 Exponential asymptotics and Stokes lines in a partial differential equation *Proc. R. Soc. A* **461** 2385–421
[3] Howls C J, Langman P J and Olde Daalhuis A B 2004 On the higher-order stokes phenomenon *Proc. R. Soc. Lond. A* **460** 2285–303
[4] Shelton J, Crew S and Trinh P H 2025 Exponential asymptotics and higher-order Stokes phenomenon in singularly perturbed ODEs *SIAM J. Appl. Math.* **85** 548–75
[5] Takei Y 2017 WKB Analysis and Stokes geometry of differential equations *Analytic, Algebraic and Geometric Aspects of Differential Equations* ed G Filipuk, Y Haraoka and S Michalik (Springer) pp 263–304
[6] Berk H L, Nevins W M and Roberts K V 1982 New Stokes' line in WKB theory *J. Math. Phys.* **23** 988–1002
[7] Arnold A 1998 Numerically absorbing boundary conditions for quantum evolution equations *VLSI Des.* **6** 313–9
[8] Arnold A and Ehrhardt M 1998 Discrete transparent boundary conditions for wide angle parabolic equations in underwater acoustics *J. Comput. Phys.* **145** 611–38
[9] Ehrhardt M and Mickens R E 2004 Solutions to the discrete Airy equation: application to parabolic equation calculations *J. Comput. Appl. Math.* **172** 183–206
[10] Tappert F D 1977 The parabolic approximation method *Wave Propagation and Underwater Acoustics* vol 70, ed J B Keller and J S Papadakis (Springer) pp 224–87
[11] Mickens R E 1993 *Nonstandard Finite Difference Models of Differential Equations* (World Scientific)
[12] Mickens R E 1997 Asymptotic properties of solutions to two discrete Airy equations *J. Differ. Equ. Appl.* **3** 231–9
[13] Bender C M and Orszag S A 2013 *Advanced Mathematical Methods for Scientists and Engineers I: Asymptotic Methods and Perturbation Theory* (*Advanced Mathematical Methods for Scientists and Engineers*) (Springer)
[14] Dingle R B 1973 *Asymptotic Expansions: Their Derivation and Interpretation* (Academic)
[15] Chapman S J, King J R and Adams K L 1998 Exponential asymptotics and Stokes lines in nonlinear ordinary differential equations *Proc. R. Soc. A* **454** 2733–55
[16] Joshi N and Lustri C J 2015 Stokes phenomena in discrete Painlevé I *Proc. R. Soc. A* **471** 20140874
[17] Wang Z and Wong R 2003 Asymptotic expansions for second-order linear difference equations with a turning point *Numer. Math.* **94** 147–94
[18] Huang X M, Lin Y and Zhao Y Q 2021 Asymptotics of the Charlier polynomials via difference equation methods *Anal. Appl.* **19** 679–713
[19] Li Y T, Wang X S and Wong R 2020 Asymptotics of the Wilson polynomials *Anal. Appl.* **18** 237–70
[20] Wang X S and Wong R 2012 Asymptotics of orthogonal polynomials via recurrence relations *Anal. Appl.* **10** 215–35
[21] Dai D, Ismail M E H and wang X S 2014 Plancherel–Rotach asymptotic expansion for some polynomials from indeterminate moment problems *Constr. Approx.* **40** 61–104
[22] Braun P A 1978 WKB method for three-term recursion relations and quasienergies of an anharmonic oscillator *Theor. Math. Phys.* **37** 1070–81
[23] Burr K P, Triantafyllou M S and Yue D K P 2000 Asymptotic analysis of wave propagation along weakly non-uniform repetitive systems *J. Sound Vib.* **229** 21–64
[24] Moston-Duggan A J, Porter M A and Lustri C J 2022 Nanoptera in higher-order nonlinear Schrödinger equations: Effects of discretization *J. Nonlinear Sci.* **33** 12
[25] Kashani-Poor A K 2016 Quantization condition from exact WKB for difference equations *J. High Energy Phys.* JHEP06(2016)180
[26] Cao L H and Li Y T 2014 Linear difference equations With a transition point at the origin *Anal. Appl.* **12** 75–106
[27] Wang Z and Wong R 2005 Linear difference equations with transition points *Math. Comput.* **74** 629–53
[28] Wong R and Li H 1992 Asymptotic expansions for second-order linear difference equations, II *Stud. Appl. Math.* **87** 289–324
[29] Wong R 2014 Asymptotics of linear recurrences *Anal. Appl.* **12** 463–84
[30] Wong R and Zhao Y Q 2022 Recent advances in asymptotic analysis *Anal. Appl.* **20** 1103–46
[31] Spigler R and Vianello M 1994 Discrete and continuous Liouville-Green-Olver approximations: a unified treatment via Volterra-Stieltjes integral equations *SIAM J. Math. Anal.* **25** 720–13
[32] Spigler R 2019 Canonical forms and discrete Liouville–Green asymptotics for second-order linear difference equations *Adv. Differ. Equ.* **2019** 361
[33] Geronimo J S and Smith D T 1992 WKB (Liouville-Green) analysis of second order difference equations and applications *J. Approx Theory* **69** 269–301
[34] Geronimo J S, Bruno O and Van Assche W 2004 WKB and Turning Point Theory for Second-order Difference Equations *Spectral Methods for Operators of Mathematical Physics* ed J Janas, P Kurasov and S Naboko (Birkhäuser Basel) pp 101–38
[35] Fedotov A A and Klopp F 2019 The complex WKB method for difference equations and Airy functions *SIAM J. Math. Anal.* **51** 4413–47
[36] Barnes E W 1904 On the homogeneous linear difference equation of the second order with linear coefficients *Messenger Math.* **34** 52–71
[37] Wimp J and Zeilberger D 1985 Resurrecting the asymptotics of linear recurrences *J. Math. Anal.* **111** 162–76
[38] Boyd W G C 1994 Gamma function asymptotics by an extension of the method of steepest descents *Proc. R. Soc.* **447** 609–30
[39] Nemes G 2015 Error bounds and exponential improvements for the asymptotic expansions of the gamma function and its reciprocal *Proc. R. Soc. Edinburgh A* **145** 571–96
[40] Howls C J, King J R, Nemes G and Olde Daalhuis A B 2025 Smoothing of the higher-order Stokes phenomenon *Stud. Appl. Math.* **154** e70008
[41] Aoki T, Kawai T and Takei Y 2001 On the exact steepest descent method: a new method for the description of Stokes curves *J. Math. Phys.* **42** 3691–713
[42] Honda N, Kawai T and Takei Y 2015 *Virtual Turning Points* vol 4 (Springer)
[43] Aoki T, Kawai T, Sasaki A, Shudo A and Takei Y 2005 Virtual turning points and bifurcation of Stokes curves for higher order ordinary differential equations *J. Phys. A* **38** 3317–36
[44] Honda N 2007 On the Stokes geometry of the Noumi–Yamada system RIMS Kôkyûroku Bessatsu B245–72
[45] Honda N 2008 The geometric structure of a virtual turning point and the model of the Stokes geometry RIMS Kôkyûroku Bessatsu B63–113

[46] Olde Daalhuis A B 2004 On higher-order Stokes phenomena of an inhomogeneous linear ordinary differential equation *J. Comput. Appl. Math.* **169** 235–46
[47] Chapman S J, Howls C J, King J R and Olde Daalhuis A B 2007 Why is a shock not a caustic? the higher-order Stokes phenomenon and smoothed shock formation *Nonlinearity* **20** 2425
[48] Body G L, King J R and Tew R H 2005 Exponential asymptotics of a fifth-order partial differential equation *Eur. J. Appl. Math.* **16** 647–81
[49] NIST Digital Library of Mathematical Functions Olver F W J, Olde Daalhuis A B, Lozier D W, Schneider B I, Boisvert R F, Clark C W, Miller B R, Saunders B V, Cohl H S, McClain M A eds Release 1.1.11 of 2023-09-15 (available at: https://dlmf.nist.gov/)
[50] King J R and Chapman S J 2001 Asymptotics beyond all orders and Stokes lines in nonlinear differential-difference equations *Eur. J. Appl. Math.* **12** 433–63
[51] Olde Daalhuis A B, Chapman S J, King J R, Ockendon J R and Tew R H 1995 Stokes phenomenon and matched asymptotic expansions *SIAM J. Appl. Math.* **55** 1469–83
[52] Huang X M, Cao L H and Wang X S 2019 Asymptotic expansion of orthogonal polynomials via difference equations *J. Approx. Theory* **239** 29–50
[53] Adriano T F, Hasmi A N, Kusdiantara R and Susanto H 2025 Exponential asymptotics of dark and bright solitons in the discrete nonlinear Schrödinger equation *Physica D* **481** 134848
[54] Geronimo J S 2009 WKB and turning point theory for second order difference equations: external fields and strong asymptotics for orthogonal polynomials *arXiv: Mathematical Physics* (arXiv:0905.1684)
[55] Fedotov A A 2022 Semiclassical asymptotics of transition matrices for difference equations with two coalescing turning points *Russ. J. Math. Phys.* **29** 467–93
[56] Fedotov A A and Klopp F 2021 WKB asymptotics of meromorphic solutions to difference equations *Appl. Anal.* **100** 1557–73
[57] Berry M V 1988 Stokes' phenomenon; smoothing a Victorian discontinuity *Math. Inst. Hautes Études Sci.* **68** 211–21
[58] Berry M V 1989 Uniform asymptotic smoothing of Stokes's discontinuities *Proc. R. Soc. A* **422** 7–21
[59] Boyd J P 1999 The devil's invention: asymptotic, superasymptotic and hyperasymptotic series *Acta Appl. Math.* **56** 1–98
[60] Roman S M and Rota G C 1978 The umbral calculus *Adv. Math.* **27** 95–188